On the robustness of a blade load-based wind speed estimator to dynamic pitch control strategies: Reply to reviewers

Marion Coquelet[1,2,3], Maxime Lejeune[1], Laurent Bricteux[2], Aemilius van Vondelen[3], Jan-Willem van Wingerden[3], and Philippe Chatelain[1]

[1]Institute of Mechanics, Materials and Civil Engineering, UCLouvain, Louvain-la-Neuve, Belgium
[2]Fluids-Machines Department, UMONS, Mons, Belgium
[3]Delft Center for Systems and Control, TU Delft, Netherlands

Correspondence: Marion Coquelet (m.coquelet@tudelft.nl)

First and foremost, we wish to thank the reviewers for their time, review, and appreciation of the work. We have addressed their comments below. We also attach the revised version of the paper at the end of this document with changes marked in color. Purple is used for Reviewer 1 and green is used for Reviewer 2.

Reviewer 1

***General comment**: The submitted article entitled "On the robustness of a blade load-based wind speed estimator to dynamic pitch control strategies" presents a numerical study on the accuracy of a wind speed estimator based on measurements of blade root bending moments in the presence of different load alleviation and wake mixing control strategies. The estimator is formulated as an Extended Kalman Filter (EKF) and uses Blade Element Momentum (BEM) theory for the state-space model. The static BEM model is modified with a first-order differential filter to account for dynamic effects in the wake development and the induction of the blades. The article is well written and easy to follow, the methodology is presented comprehensively, and the results are discussed rigorously. The subject of pitch control strategies under wake conditions is also a highly relevant topic and fits the scope of this journal. Some points could benefit from further clarification.*

We thank Reviewer 1 for this excellent summary of the paper and for their appreciation of the work. We clarify the discussion points highlighted by Reviewer 1 hereunder.

***Comment 1** : The proposed approach of blade loads-based wind estimation is presented as an alternative to LIDAR measurements. Can you comment on the advantages and disadvantages of each approach? It is mentioned that LIDARs are not widely used commercially due their high capital and operational costs, but the same applies to blade Structural Health Monitoring systems (SHM). Measurements of the blade root bending moments are typically only available for modern offshore wind turbines, which limits the applicability of the proposed approach. Furthermore, there are distinctions in the prediction horizon of wind speeds. LIDARs are able to measure the upstream wind speeds and give the controller several seconds to react to the incoming wind, while blade measurements only provide estimates of current wind speeds.*

We clarify the distinctions between our proposed estimator and other measurement methods, typically LiDARs, and fully agree when it comes to the prediction horizons. Regarding the cost of LiDARs vs SHM, it is not easy to find precise numbers in the literature, but these two documents provide orders of magnitude: $\mathcal{O}(10\text{k€})$ for SHM (McGowin, 2010) and $\mathcal{O}(100\text{k€})$ for LiDARs (Canet et al., 2021). McGowin (2010) is a rather old reference, so one could imagine that the technology has become popularized and than cheaper, even if inflation might also have led to a price increase. We do not make further economical projections as this is not our scope of expertise. Nevertheless, these two documents, alongside information we have obtained from industrial partners, suggest that, currently, LiDARs are still an order of magnitude more expensive than SHM.
We adapt the Abstract and the related paragraphs of Section 1: “Introduction” as follows to clarify the message.

“In the context of wind turbine pitch control for load alleviation or active wake mixing, it is relevant to provide the time- and space-varying wind conditions as an input to the controller. Apart from classical wind measurement techniques, blade load-based estimators can also be used to sense the incoming wind. These consider blades as sensors of the flow, and rely on having access to the operating parameters and measuring the blade loads.”

“Anemometers have been present on nacelles for many years (Smith et al., 2002). Yet, they only provide information on the wind at the measurement point, making turbines unaware of wake impingement, shear or turbulent gusts. Their measurements additionally suffer from a number of disturbances resulting in unreliable measurements (Bottasso et al., 2018). Consequently, nacelle-mounted LiDARs have received growing attention, as they provide solutions to these limitations. They offer remote sensing and are able to provide a great characterization of the incoming flow. Most importantly, LIDARs are able to measure the incoming flow further upstream from the turbine, hence allowing the controller to prepare for future flow variations. For this reason, LiDARs are good candidates for feedforward control approaches (Letizia et al., 2023; Scholbrock et al., 2016). They are not a standard yet for modern turbines, likely due to their cost, complexity of installation, or need for synchronization with the SCADA system. However, their industrial use has been reported (Raach, 2021) and is likely to generalize in the future.

Alternative methods to characterize the inflow have also been investigated. They are based on the principle that any change in the wind is reflected on the load response of the rotor and that load sensors are now typically available for modern turbines (Cooperman and Martinez, 2015; Bottasso et al., 2018). This is referred to as the rotor-as-a-sensor approach, for which the structural response of the turbine is used to determine the wind conditions. Conversely to LiDARS, such approaches do not offer a preview of the future incoming wind, the estimation is limited to the current wind conditions.”

***Comment 2** : The analysis demonstrated that the modification of the BEM model could account for dynamic effects in the aerodynamics such as wake development and blade induction, however, the structural dynamics of the rotor were not considered in this study, since both the EKF estimator and the LES simulations assume a rigid rotor. In reality, the relationship between blade root measurements and wind speeds is also affected by the elastic edge- and flap-wise bending of the blades. Can you comment on how the structural dynamics would affect the accuracy of the estimator and whether the proposed BEM* *modification could account for these dynamics? Have you considered numerical studies with aeroelastic software such as OpenFAST or HAWC2 to investigate the effects of the structural dynamics?*

The structural dynamics of the rotor are indeed not considered in this study, as both the Extended Kalman Filter (EKF) estimator and the Large-Eddy Simulation (LES) simulations assume a rigid rotor. Lejeune et al. (2022) used the same estimator to infer flow information to a meandering-capturing wake model. Though not reported in their paper, they verified that providing bending moment signals from LES with flexible blades did not lead to a loss of accuracy for the estimator. Yet, as in this work, Lejeune et al. (2022) considered the NREL 5MW wind turbine, whose flexibility is limited. It is known that larger turbines are more prone to flexibility effects, with higher bending relative to the radius and a significant torsion angle (Trigaux et al., 2024a). Attention should be paid when the estimator is used for larger rotors.

Looking at the literature provides us with first intuitions about how the structural dynamics would affect the accuracy of the estimator. Accounting for blade flexibility in the LES, i.e. having more fidelity, modifies the blade root moments in three ways: mean value, amplitude of the fluctuations and phase of the fluctuations (Trigaux et al., 2024b).

Including flexibility leads to lower mean values, due to the deflection of the blade tip. This could lead to additional bias, but methods to correct for it have been mentioned in the paper.

The amplitude of the fluctuations also decreases when flexibility is accounted for, and phase lag appears (Trigaux et al., 2024b). Whether the proposed BEM modification could account for these structural dynamics is an interesting question. The current modification, based on the work of Snel and Schepers (1995), consists in filtering the induced velocities using two first-order differential equations. This leads to a low-pass filter effect on the loads (see Fig. 6), with a reduction of amplitude and a phase delay. This being the same trend as the one observed with flexibility, which results in structural damping, it would be worth investigating whether such a model can also be used to somewhat account for structural dynamics in the BEM.

We synthetize the key elements of this discussion as a perspective in Section 5: “Conclusions”.

“Another perspective is to investigate the effects of blade flexibility on the proposed estimator. The structural dynamics of the rotor are indeed not considered in this study, as both the EKF estimator and the LES simulations assume a rigid rotor. Accounting for blade flexibility modifies the blade root moments in three ways: mean value, amplitude of the fluctuations and phase of the fluctuations (Trigaux et al., 2024b). And these effects increase as the rotor diameter increases (Trigaux et al., 2024a). Further investigations are thus needed in that field, especially when the estimator is used for larger rotors.”

Comment 3 *: Fig 5,6: the y-axis description seems to be corrupted.*

Thank you for pointing this out, it will be corrected in the revised manuscript.

Comment 4 *: How are the covariance matrices Q and R of the EKF determined? Was the EKF tuned with respect to Q and R?*

Several combinations of process noise covariance and measurement noise covariance are tested to determine the best configuration. Figure 1 of this document shows the sensitivity of the estimate to the covariances. It shows that high Q/R ratios lead to reduced estimation errors and that R should remain small to avoid excessive filtering and hence delay. In this case,

$Q^* = Q/(U^*)^2 = \mathcal{O}(0.1)$ and $R^* = R/(M_n^*)^2 = \mathcal{O}(0.0001)$, where U^* and M_n^* represent the order of magnitude of the incoming wind speed and bending moments, respectively.

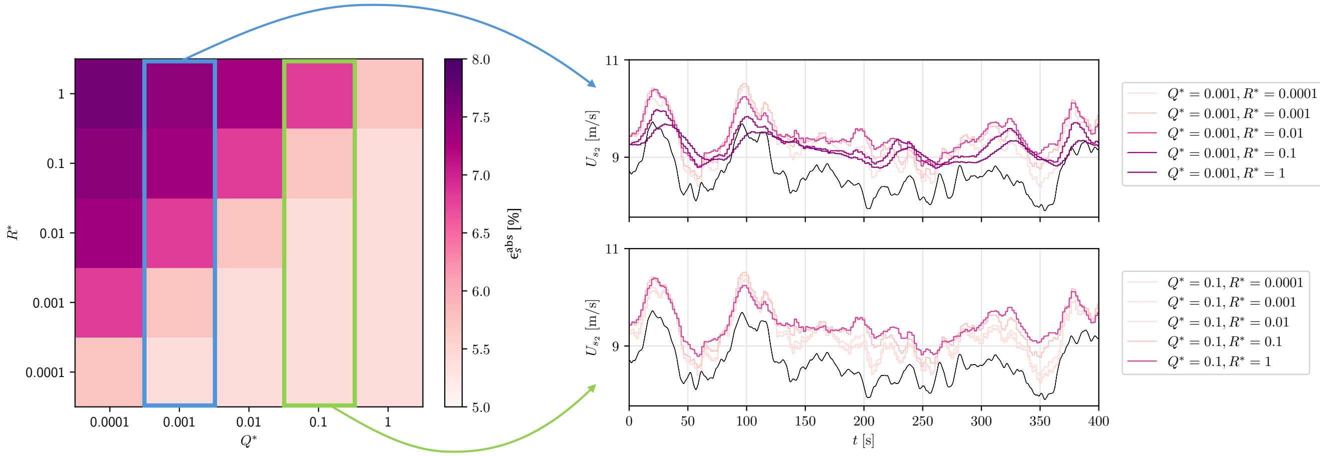

Figure 1. Sensitivity of the estimate to the values of Q and R: Estimate error for the sector-effective wind speeds depending on the value of Q^* and R^* (left) and time series of the sector-effective wind speeds (right), black is the reference wind speed extracted from the LES and the colored lines represent the estimates, they are colored by the error.

This precision is included in Section 2.1.2: "Estimation of blade-effective wind speeds".

*"**Noise covariance matrices**: Several combinations of process noise covariance and measurement noise covariance are tested to determine the best configuration. The values leading to the smallest estimation errors and avoiding excessive filtering are $Q^* = Q/(U^*)^2 = 0.1$ and $R^* = R/(M_n^*)^2 = 0.0001$, where U^* and M_n^* represent the order of magnitude of the incoming wind speed and bending moments, respectively."*

***Final comment**: Overall, the submitted article is of high quality and I recommend the publication once the above comments have been addressed adequately.*

We wish to thank Reviewer 1 again for their general appreciation of the work, and also for highlighting discussion points. We hope to have addressed the above comments adequately, as we believe they contribute to improving the quality of the paper.

Reviewer 2

General comment*: This is a very well-written, clearly explained paper that addresses the accuracy of blade-load based wind speed estimators when pitch control strategies with high pitching frequencies are used. This is a relevant topic because of the interest in using rotor-based wind estimates as part of individual pitch controllers or active wake mixing control strategies. The methodology of evaluating the estimators using high-fidelity modeling that is largely independent of the BEM models used in the estimator makes for a robust analysis of estimator accuracy. Finally, the use of a model of the induced velocity dynamics, which has been used for rotor effective wind speed estimators in the past, is a novel contribution to the field of blade load-based wind speed estimation.*

We thank Reviewer 2 for their enthusiastic and positive appreciation of this paper. We appreciate their feedback, as including it to the revised version of the paper provides additional value to the work.

There are no major issues with the paper, but in the list below are several mostly small comments that I believe should be addressed. The main comments include a) describing how the reference wind variables to which the estimates are compared are calculated, b) clarifying why the spatial filtering inherent in the blade-load based estimates could be a significant source of estimation error, since the reference variables should also include spatial filtering, c) providing results in Section 4 for above-rated operation where collective pitch control is active to give a more complete picture of the estimator accuracy and potential need for dynamic BEM models during all pitch control scenarios.

These main remarks are addressed by replying to the dedicated comments hereunder: a) the reference wind variables calculation is presented in the response to ***Comment 6***, b) what is understood by filtering is clarified in the response to ***Comment 10***, c) results for above-rated operation are provided in the response to ***Comment 18***. The other small comments are also addressed hereunder.

Comment 1 *: Ln. 33: "Information on the flow conditions, whether explicitly or through blade loads, is not used." This is a little misleading because wake mitigation controllers should at least use measurements/estimates of the wind speed and direction and determine the specific control actions based on whether there are any downstream turbines that would benefit from wake mitigation.*

We agree with this comment and modify the related paragraphs of Section 1: "Introduction" as follows.

"When it comes to dynamic wake mixing, the Pulse and the Helix strategies act in an open-loop manner. In previous experimental and numerical contributions (van der Hoek et al., 2024; Korb et al., 2023), the pitch actuation frequency is fixed for a studied configuration. It is computed based on the mean infinite upstream wind speed to match a chosen Strouhal number."

Comment 2 *: Section 2.1.2: "Estimation of blade-effective wind speeds": What is the sampling time/update rate of the EKF blade-effective wind speed estimator?*

The "measurements" of the bending moments are provided by the LES, hence the update rate for the blade-effective wind speed estimates cannot be higher than the LES time step. For the simulations presented in Section 3: "Validation of the estimator", the LES time step depends on the upstream wind speed and is adaptive. The operating parameters of the turbine are resampled at a 10 Hz frequency to feed the EKF, so the EKF time step is 0.1 s. For the simulations presented in Section 4: "Robustness of the estimation", the LES time step is fixed at 0.1 s and so is the EKF time step.

Modification in Section 3.1: "Numerical setup":

"The LES time step is adaptive and the operating parameters of the turbine are sampled at a 10 Hz frequency to feed the EKF."

Modification in Section 4.2: "Numerical setup":

"The wind speed estimation for both the upstream and the downstream turbine is performed at a 10 *Hz frequency."*

***Comment 3** : Fig. 1 is missing some characters in the output variable names on the right side.. Similarly, Figs. 2, 5, 6, 7, and 8 are missing some characters in the axis labels (and for Figs. 5 and 6 the titles as well).*

Thank you for pointing this out, it will be corrected in the revised manuscript.

***Comment 4** : Ln. 150: "We model the system using the BEM theory": Do you use a specific BEM software, or have you written your own implementation?*

The BEM used in this work was implemented in-house following Hansen (2015) and validated against FAST. This precision is included in Appendix A: "Blade Element Momentum theory".

"The BEM used in this work was implemented in-house following Hansen (2015) and validated against FAST. Rotor tilt and blade cone angle are not taken into account, the rotor is considered as a flat disk perpendicular to the inflow."

***Comment 5** : Ln. 179: "r = 2R/3": Can you explain the motivation for assuming the sector-effective wind speeds represent the wind at this radial location?*

This assumption is explained in Bottasso et al. (2018), see Fig. 2 of this document. We add the reference in Section 2.1.3: "Reconstruction of the incoming wind".

"Following derivations in Bottasso et al. (2018), sector-effective wind speeds are assumed to account for the wind speed at $r = 2R/3$*."*

***Comment 6** : Section 3.2: Please describe how the true values of the estimated variables are determined from the adjunct LES. For example, are sector wind speeds calculated by averaging the longitudinal u component of wind over the sector areas? Is shear determined by fitting to the sector average wind speeds or by finding the best-fit shear over the entire rotor area?*

The blade root bending moment on a sector S occupying the azimuthal span $\Delta\psi = \psi_2 - \psi_1$ with area $A_S = \Delta\psi R^2/2$ can be written as

$$m_S = \frac{1}{2B}\rho R^3 \int_0^1 \int_{\psi_1}^{\psi_2} V(\xi,\psi)^2 C_T(\xi,\psi)\xi^2 \, \mathrm{d}\psi \mathrm{d}\xi, \tag{13}$$

where $\xi = r/R$ is the nondimensional radial position, r the dimensional one, and C_T the local thrust coefficient. According to stream-tube theory, $C_T(\xi) = 4a(\xi)(1-a(\xi))$, where $a(\xi)$ is the axial induction factor. As $a(\xi) \approx 1/3$ for a well designed blade, then C_T can be assumed to be roughly constant over the rotor disk. Therefore, introducing the constant equivalent wind speed V_{SE} over the sector, one readily finds

$$m_S = \frac{1}{2B}\rho V_{SE}^2 A_S \frac{2}{3} R C_T. \tag{14}$$

This expression indicates that the blade bending moment can be interpreted as being produced by the thrust applied at $2R/3$ span. In this sense, V_{SE} can be interpreted as the wind velocity sampled at that same location.

Figure 2. Extract of Bottasso et al. (2018) on assuming the sector-effective wind speeds represent the wind at $r/R = 2/3$.

We added the description of how reference wind speeds are computed in Section 3.1: "Numerical setup".

"An adjunct LES in which no turbine is present is also performed for each wind case. The quantities estimated by the EKF can then be assessed by comparing them to the "ground truth", as the additional simulations provide an unambiguous definition of the freestream quantities. The rotor-effective wind speeds are computed as the average, over a disk located at the position of the rotor in the original simulation, of the streamwise velocity extracted from the adjunct LES. This is formally computed as

$$U_{r,k}^{\mathrm{LES}} = \frac{1}{\pi R^2} \iint_{\mathrm{disk}} u_{x,k}(x = x_{WT}, y, z)\, \mathrm{d}S, \tag{1}$$

where $u_{x,k}$ is the streamwise velocity field at time k, x_{WT} is the location of the wind turbine in the original simulation and the spatial integral is performed over the disk area swept by the rotor blades. The formulation for the sector-effective wind speeds is similar, except for the fact that the spatial integral is performed over each sector area, such that

$$U_{s,k}^{\mathrm{LES}} = \frac{n_S}{\pi R^2} \iint_{\mathrm{sector}} u_{x,k}(x = x_{WT}, y, z)\, \mathrm{d}S. \tag{2}$$

The tilt and yaw shear coefficients, $\alpha_{\mathrm{tilt},k}^{\mathrm{LES}}$ and $\alpha_{\mathrm{yaw},k}^{\mathrm{LES}}$ are retrieved from the sector-effective wind speeds using the least square fit approach as described in Eq. 17. The quantities estimated by the EKF can then be assessed by comparing them to the values recovered from the adjunct LES, which provides an unambiguous definition of the freestream quantities."

***Comment 7** : Ln. 215: What is the time step used?*

See reply to Comment 2.

Comment 8 *: Eqs. 18-20: Please define "U_{ref}"*

U_{ref} is the mean infinite upstream wind speed. This is now specified is Section 3.1: "Numerical setup".

"For this validation study, we consider mean infinite upstream wind speeds U_{ref} of 5 m/s, 9 m/s and 14 m/s and turbulence intensity (TI) of 6%, 10% and 15%, hence 9 wind cases are considered."

Comment 9 *: Eqs. 21 and 22: What is the variable $\alpha_{h,k}$? Should this be $\alpha_{yaw,k}$ and $\alpha_{tilt,k}$?*

This is a typo, it should indeed be $\alpha_{\text{yaw},k}$ and $\alpha_{\text{tilt},k}$. We have corrected it.

Comment 10 *: Pg. 9, 1st sentence: "We attribute this to the inherent spatial filtering introduced by the blade-as-a-sensor approach.": Can you explain this in more detail? It seems like the true values of the variables to which the estimates are compared would also include spatial filtering (if they are calculated as the spatial average over the sector areas), so the spatial filtering due to the blade should be beneficial in matching the true rotor effective wind speeds, sector wind speeds, and effective shears.*

We agree that the formulation of this sentence is unclear and misleading. We clarify our point in Section 3.2: "Results".

"We relate this to the spatio-temporal averaging underlying the estimation process. The reference sector-effective wind speed is the unweighted average of the flow field in the radial and azimuthal directions. The sector-effective wind speed estimated by the EKF is also the result of an averaging, but the latter is performed differently. First, the radial averaging is materialized by the blade-effective wind speed. The latter is computed by the EKF as to minimize the difference between the measured bending moment (here extracted from LES) and the modeled bending moment (here obtained from the Blade Element Momentum (BEM)). So the EKF uses the BEM to synthesize a turbulent wind speed distribution into a single blade-effective wind speed. Yet a wind turbine blade, and as a consequence the BEM, is nonlinear. Therefore the radial averaging is not simply an unweighted average. Second, the azimuthal averaging is performed by the transformation from blade-effective wind speed to sector-effective wind speed. Every azimuthal data considered to get the sector average is taken at a different instant and the estimated sector-effective wind speed is only updated at a 3P frequency. This is the limitation of using discrete blades as sensors. To summarize, the reference sector-effective wind speed at time t is a linear combination of local wind speeds at time t, while the estimated sector-effective wind speed at time t is a non linear combination of local wind speeds from time $t - T_{rot}/3$ to t. If the flow field was uniform, the averaging performed by the estimator would be equivalent to the reference averaging. But as turbulence increases, the output of the spatio-temporal filtering associated with the estimator diverges from the reference."

Comment 11 *: Ln. 263: "eventually forcing the wake to displace laterally (see Fig. 3)..": Should this be "laterally and vertically"?*

We changed this in the revised version.

Comment 12 *: Ln. 281: Similar to comment 6, how are the reference velocities calculated?*

The reference velocities are computed following Eq. 19 and Eq. 20. This is included at the end of Sec. 4.2 Numerical setup.

Comment 13 *: Ln. 282 and 283: I believe (Fig. 4(b)) and (Fig. 4(c)) in the text should be changed to (Fig. 4(a)) and (Fig. 4(b)). In this case Fig. 4(c) may need to be referenced in the text elsewhere.*

We modified this in the revised version and included a reference to Fig. 4(c) in the text.

Comment 14 *: Fig. 4 caption: "used as reference wind speeds to verify it": To verify what? Consider something like "to verify the estimated values".*

We modified the caption as follows: *"used as reference to verify the wind speeds estimates for the first and second turbines."*

Comment 15 *: Eq. 24: Should "w_{qs}/dt" be changed to "dw_{qs}/dt"?*

It should indeed, the typo has been corrected.

Comment 16 *: Eqs. 27-30: This section suggests that the induced velocity filtering time constants are specific to the type of control strategy. Can you comment on how these should be tuned for a turbine that uses IPC some of the time, helix (or another wake mixing control strategy) sometimes, and also collective pitch control for rotor speed regulation? Would you need to be updating the time constants frequently during operation based on the current control mode, or would you use one value that works reasonably well for all cases? Lastly, if only collective pitch control for rotor speed regulation is used, how would you determine the pitching frequency value?*

The estimator should adapt its time constants based on the current control mode. The time constants can be set to zero for Baseline and IPC approaches, as the paper shows that filtering for the induced velocities in the BEM is only needed when dynamic wake mixing control is used. For the Pulse or the Helix, only the pitching frequency is required to compute the time constants (see Eq. 30 and Eq. 31), and this information is known to the controller. Using the same time constant for Helix and Pulse is not an option, as the pitching frequencies are one order of magnitude apart. It was unsuccessfully tested, as Fig. 3 of this documents reveals.

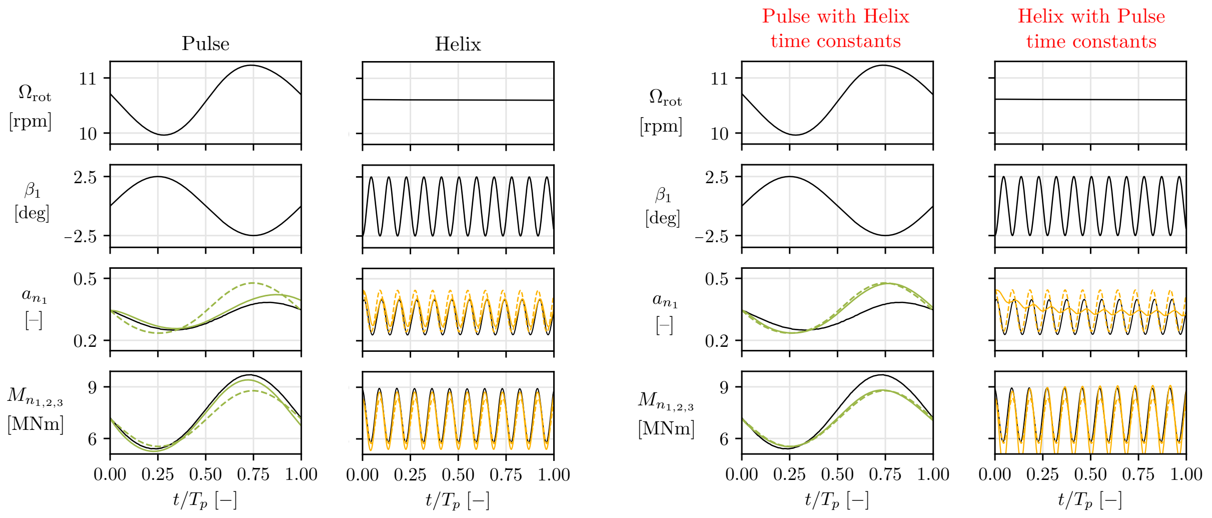

Figure 3. Comparison of LES (solid black), static BEM (dashed colored) and dynamic BEM (solid colored) in the evaluation of the local forces acting on the airfoil located at $r/R = 3/4$ for the NREL 5MW operated in uniform flow with $U_{\mathrm{ref}} = 9$ m/s.

Comment 17 *: Section 4.5: If possible, it would be useful to show the accuracy of the best-fit horizontal and vertical shear in addition to the sector wind speeds and rotor effective wind speeds, as in Section 3, because these quantities could be used to inform IPC control strategies.*

This is now included in Fig. 9, Section 4.4: "Above-rated conditions: 14 m/s". See reply to Comment 18 hereunder.

Comment 18 *: Section 4.5 and 4.6: If possible, it would be valuable to show results for an above-rated wind speed (like 14 m/s as in Section 3) in addition to the 9 m/s case. First, IPC for load reduction is more commonly used in above-rated conditions, so it would be useful to show the estimator accuracy with IPC during above-rated operation. Second, because collective pitch control for rotor speed regulation is active in above-rated wind speeds but not in below-rated conditions around 9 m/s, it would be important to understand whether the static BEM-based estimator is sufficient when only collective pitch control is used, or if dynamic BEM is needed in this case too.*

This case is indeed relevant, hence we have added the simulations of the Baseline and Individual Pitch Control (IPC) control cases at 14 m/s. Results show that the static BEM is sufficient in those cases as no rapid changes in induction are associated with these two control cases. It also shows that the bias of the estimator decreases, as the BEM is more reliable at higher wind speeds. Section 4.2: "Numerical setups" was modified to introduce these new cases and Section 4.4: "Above-rated conditions: 14 m/s" gathers these new results and is copied hereunder.

"The inflow wind is sheared ($\alpha = 0.2$) and turbulent ($TI = 6\%$), in order to represent atmospheric boundary layer flows. Two wind speeds are considered: 9 m/s and 14 m/s. For the 9 m/s cases, both turbines operate in under-rated conditions: this

is representative of a configuration in which wake mixing control would be applied. On the first turbine, we therefore test the Baseline controller, the Pulse, the Helix and IPC for the sake of completeness, even though it is usually not used at below-rated wind speeds. The downstream turbine is always operated using the Baseline controller. We opt for commonly used parameters for both the Helix and the Pulse (Frederik et al., 2020; Munters and Meyers, 2018): $St = 0.25$ and $A = 2.5^{\circ}$. Note that, as both turbines operate at under-rated wind speed, only the generator torque control is active for the Baseline controller, such that the collective pitch control $\beta_{coll} = 0$. For the 14 m/s cases, both turbines operate in above-rated conditions. There would be no point in using wake mixing control in that case, hence it is not tested. Conversely, this is a configuration in which both the upstream and downstream turbines would use load alleviation control. We therefore consider two cases: Baseline controller on both turbines and IPC on both turbines. In both cases, collective pitch control is used by the Baseline controller for power regulation. When load alleviation control is switched on, the individual pitch commands are added on top of the collective pitch command, following the Coleman transform. Table 1 summarizes the above-mentioned cases."

9 m/s		14 m/s	
WT1	WT2	WT1	WT2
Baseline	Baseline	Baseline	Baseline
IPC	Baseline	IPC	IPC
Helix	Baseline		
Pulse	Baseline		

Table 1. Summary of the configurations tested to investigate the robustness of blade-load based estimator to active pitch control.

" This final section discusses the above-rated wind speed cases. The impact of using IPC on the pitch angle and blade loads was highlighted in Fig. 5 and is not shown here anymore. Note however that Collective Pitch Control (CPC) is active in these wind conditions. Figure 4 shows the time series of the wind speed estimates for the two turbines. The static BEM is used as internal model. Separate subfigures are used for the downstream turbine as the wake is slightly different whether IPC is used on the upstream turbine or not (Wang et al., 2020). The reference wind speed is thus slightly different for the two cases, as it can be observed when carefully looking at Fig. 4. Instead of showing all sector-effective wind speeds as in the previous sections, Figure 4 rather presents the horizontal and vertical shear coefficient, as these quantities are specifically insightful for load alleviation control using IPC. First, results show that the static BEM is sufficient in these cases. CPC for power regulation is active in the Baseline case and additional individual pitching is added on top of it in the IPC case. Still, no rapid changes in induction are associated with the two control cases, hence the static BEM is accurate to model the link between operating parameters, wind speed and blade bending moments.

Figure 4 also shows that the bias of the estimator is reduced, both for the freestream and the waked turbine. This is quantitatively confirmed by Table 2, which shows that errors remain under 3% for the estimated wind speeds. It is a direct consequence of the higher wind speed: the BEM is more accurate at reduced thrust coefficients, i.e. at higher wind speeds, hence the esti-

mation is better. Time series also show a good capture of the shear coefficients. The vertical wind shear of the inflow is sensed (α_{tilt} is non zero on average), while the horizontal shear generated by gusts is also seen (α_{yaw} varies around a zero mean).”

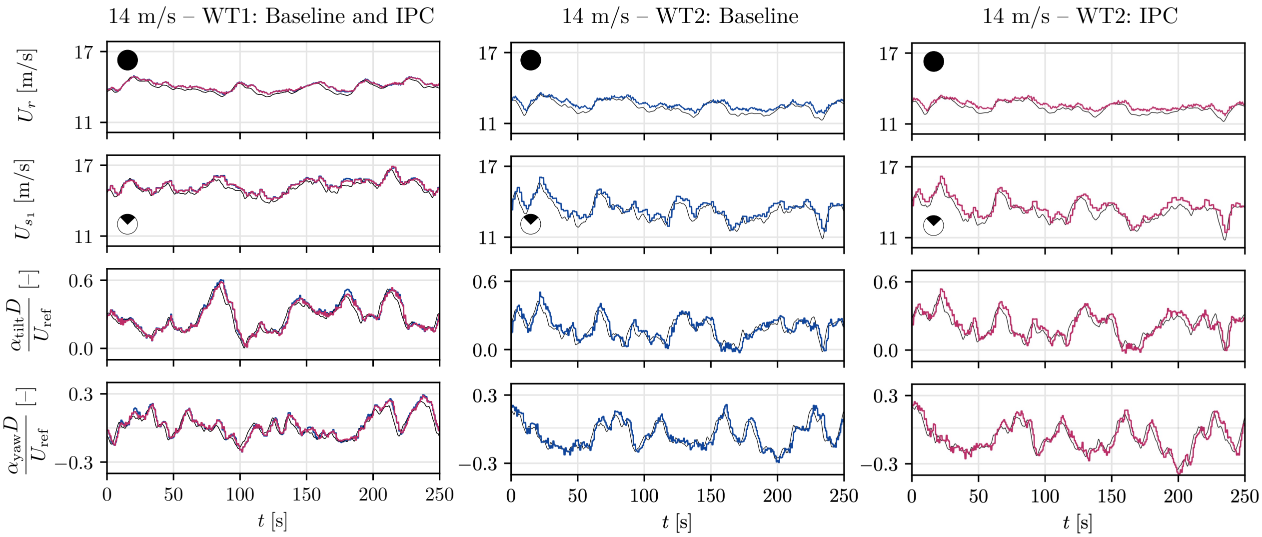

Figure 4. 14 m/s case: Time series of estimated wind speeds for both turbines (WT1 and WT2), using a static BEM as internal model in the EKF. Reference velocities (black) are extracted from the LES, both turbines are either operated with Baseline (blue) or IPC (red).

	Baseline WT1	IPC WT1	Baseline WT2	IPC WT2
$\epsilon^{\text{abs}}_{U_r}$ [%]	1.4	1.4	1.8	1.8
$\epsilon^{\text{abs}}_{U_s}$ [%]	2.0	2.0	2.5	2.6
ϵ_{U_s} [%]	1.5	1.5	1.9	2.0
$\epsilon_{\alpha_{\text{tilt}}}$ [%]	11.0	10.9	20.2	20.7
$\epsilon_{\alpha_{\text{yaw}}}$ [%]	17.7	17.1	17.7	16.1

Table 2. 14 m/s case: Wind speeds and shear coefficients estimation errors for the two turbines (WT1 and WT2). The latter are either both operated with Baseline control or with IPC.

Comment 19 *: Tables 2 and 3: Can you comment on why the estimation errors are slightly higher when only baseline control is used rather than the more complex IPC and wake mixing controllers?*

First, it would be interesting to collect longer statistics or run simulations with several turbulent seeds to verify whether a trend really is present or not. In the case the trend holds, we would investigate the following hypotheses. When IPC is used, the 1P variations of the blade loads are attenuated. In terms of blade aerodynamics, it means that angles of attack are kept more constant over the blade rotation. We have seen that this limits, to some extent, the amplitude of the 1P variations of the axial induction factor. This could lead to the BEM being slightly more accurate in the IPC case than in the Baseline one. For the wake mixing cases, the time constants of the dynamic BEM have been tuned to match the LES force variations associated with the pitching. This could be responsible for a more accurate model than in the Baseline case.

Comment 20 *: Ln. 382:"likely also due to the filtering effect of the blade-to-sector conversion." Same as comment 10, my understanding is that the reference variables to which the estimates are compared also include spatial filtering. In this case, how would the spatial filtering of the estimator vs. the ground-truth references differ and thus contribute to estimation error?*
See reply to comment 10.

Comment 21 *: Appendix A: Does the BEM model account for the rotor tilt and cone angle? Or is the rotor approximated as being perpendicular to the inflow?*
The rotor is approximated as being perpendicular to the inflow. This precision is included in Appendix A: "Blade Element Momentum theory".

"The BEM used in this work was implemented in-house following Hansen (2015) and validated against FAST. Rotor tilt and blade cone angle are not taken into account, the rotor is considered as a flat disk perpendicular to the inflow."

Comment 22 *: Algorithm A1: This is a nice presentation of the BEM algorithm. Could you also provide the tolerance value you use?*
Thank you for your appreciation. The tolerance is set on the flow angle ϕ and not the axial induction a as suggested in the pseudo-algorithm included in the original version. We modify the pseudo-algorithm to highlight that the tolerance refers to ϕ. Here it is set to $\mathrm{tol} = 10^{-6}$. We also include this precision in Appendix A: "Blade Element Momentum theory".

Comment 23 *: Algorithm B1: This algorithm is relatively easy to follow, but a couple variables could be clarified. Could you explain $\Delta\theta$ and just to perfectly clear "n_B"?*
We updated the text of Appendix B: "From blade-effective wind speed to sector-effective wind speed" as follows.

"The rotor swept area is divided into n_S sectors of azimuthal span $\Delta\theta = 2\pi/n_S$. Algorithm B2 formalizes the conversion from blade-effective wind speed ($U_{b,k}$) to sector-effective wind-speed ($U_{s,k}$) for a rotor with n_B blades. The second subscript stands for the time index k. The process is initiated at $k = 1$ for each blade b by determining the sector $s_{b,k=1}$ in which the blade is located based on its azimuthal position $\theta_{b,k=1}$. History of blade-effective wind speed is then accumulated while the blade is passing through the sector using the counting variable nit_b. The sector-effective wind speed of sector s is eventually updated when the blade leaves the sector $s_b = s$. While the blade-effective wind speeds are updated at every time index k, i.e. at the EKF estimation frequency ($0.1\,\mathrm{s}$ in this work), the sector-effective wind speeds are only updated at a 3P frequency (around $2\,\mathrm{s}$) in this context."

References

Bottasso, C., Cacciola, S., and Schreiber, J.: Local wind speed estimation, with application to wake impingement detection, Renewable Energy, https://doi.org/10.1016/j.renene.2017.09.044, 2018.

Canet, H., Loew, S., and Bottasso, C. L.: What are the benefits of lidar-assisted control in the design of a wind turbine?, Wind Energy Science, 6, 1325–1340, https://doi.org/10.5194/wes-6-1325-2021, 2021.

Cooperman, A. and Martinez, M.: Load monitoring for active control of wind turbines, Renewable and Sustainable Energy Reviews, 41, 189–201, https://doi.org/https://doi.org/10.1016/j.rser.2014.08.029, 2015.

Frederik, J., Doekemeijer, B., Mulders, S., and van Wingerden, J.W.: The helix approach: Using dynamic individual pitch control to enhance wake mixing in wind farms, Wind Energy, https://doi.org/10.1002/we.2513, 2020.

Hansen, M.: Aerodynamics of wind turbines, Routledge, 2015.

Korb, H., Asmuth, H., and Ivanell, S.: The characteristics of helically deflected wind turbine wakes, Journal of Fluid Mechanics, 965, A2, https://doi.org/10.1017/jfm.2023.390, 2023.

Lejeune, M., Moens, M., and Chatelain, P.: A meandering-capturing wake model coupled to rotor-based flow-sensing for operational wind farm flow prediction, Frontiers in Energy Research, https://doi.org/10.3389/fenrg.2022.884068, 2022.

Letizia, S., Brugger, P., Bodini, N., Krishnamurthy, R., Scholbrock, A., Simley, E., Porté-Agel, F., Hamilton, N., Doubrawa, P., and Moriarty, P.: Characterization of wind turbine flow through nacelle-mounted lidars: a review, Frontiers in Mechanical Engineering, 9, https://doi.org/10.3389/fmech.2023.1261017, 2023.

McGowin, C.: Wind Turbine Blade Structural Health Monitoring, Tech. rep., Electrical Power Research Institute (EPRI), 2010.

Munters, W. and Meyers, J.: Towards practical dynamic induction control of wind farms: analysis of optimally controlled wind-farm boundary layers and sinusoidal induction control of first-row turbines, Wind Energy Science, https://doi.org/10.5194/wes-3-409-2018, 2018.

Raach, S.: Important milestone: 1000 wind turbines with lidar-assisted control, Sowento, https://www.sowento.com/wp-content/uploads/2021/11/20210527-sowento-PressRelease-Goldwind.pdf, 2021.

Scholbrock, A., Fleming, P., Schlipf, D., Wright, A., Johnson, K., and Wang, N.: Lidar-enhanced wind turbine control: Past, present, and future, in: 2016 American Control Conference (ACC), pp. 1399–1406, IEEE, https://doi.org/10.1109/ACC.2016.7525113, 2016.

Smith, B., Link, H., Randall, G., and McCoy, T.: Applicability of nacelle anemometer measurements for use in turbine power performance tests, Tech. rep., National Renewable Energy Laboratory (NREL), 2002.

Snel, H. and Schepers, J.: Joint investigation of dynamic inflow effects and implementation of an engineering method, in: 1993 ECWEC Conference, ECWEC, 1995.

Trigaux, F., Chatelain, P., and Winckelmans, G.: Investigation of blade flexibility effects over the loads and wake of a 15 MW wind turbine using a flexible actuator line method, Wind Energy Science Discussions, 2024, 1–33, https://doi.org/10.5194/wes-2024-19, 2024a.

Trigaux, F., Chatelain, P., and Winckelmans, G.: Investigation of blade flexibility effects over the loads and wake of a 15 MW wind turbine using a flexible actuator line method, Wind Energy Science Discussions, 2024, 1–33, https://doi.org/10.5194/wes-2024-19, 2024b.

van der Hoek, D., den Abbeele, B. V., Simao Ferreira, C., and van Wingerden, J.-W.: Maximizing wind farm power output with the helix approach: Experimental validation and wake analysis using tomographic particle image velocimetry, Wind Energy, 27, 463–482, https://doi.org/10.1002/we.2896, 2024.

Wang, C., Campagnolo, F., and Bottasso, C.: Does the use of load-reducing IPC on a wake-steering turbine affect wake behavior?, Journal of Physics: Conference Series, https://doi.org/10.1088/1742-6596/1618/2/022035, 2020.

On the robustness of a blade load-based wind speed estimator to dynamic pitch control strategies

Marion Coquelet[1,2,3], Maxime Lejeune[1], Laurent Bricteux[2], Aemilius van Vondelen[3], Jan-Willem van Wingerden[3], and Philippe Chatelain[1]

[1]Institute of Mechanics, Materials and Civil Engineering, UCLouvain, Louvain-la-Neuve, Belgium
[2]Fluids-Machines Department, UMONS, Mons, Belgium
[3]Delft Center for Systems and Control, TU Delft, Netherlands

Correspondence: Marion Coquelet (m.coquelet@tudelft.nl)

Abstract. In the context of wind turbine pitch control for load alleviation or active wake mixing, it is relevant to provide the time- and space-varying wind conditions as an input to the controller. Apart from classical wind measurement techniques, blade load-based estimators can also be used to sense the incoming wind. These consider blades as sensors of the flow, and rely on having access to the operating parameters and measuring the blade loads. In this paper, we wish to verify how robust such estimators are to the control strategy active on the turbine, as it impacts both operating parameters and loads. We use an Extended Kalman Filter (EKF) to estimate the incoming wind conditions based on the blade bending moments. The internal model in the EKF relies on the Blade Element Momentum (BEM) theory in which we propose to account for delays between pitch action and blade loads by including dynamic effects. Using Large-Eddy Simulations to test the estimator, we show that accounting for the dynamic effects in the BEM formulation is needed to maintain the estimator accuracy when dynamic wake mixing control is active.

1 Introduction

With their 2030 Agenda for Sustainable Development, the United Nations (2015) set 17 Goals to ensure Sustainable Development of our planet. Sustainable Development Goal number 7 aims at ensuring access to affordable, reliable, sustainable and modern energy for all. In that perspective, reducing the Levelized Cost of Energy (LCoE) coming from wind is essential. Two factors contributing to this effort are considered here: increasing wind farm power capture and reducing the occurrence of turbine failures. Wind turbine and wind farm flow control can contribute to these two objectives.

Individual Pitch Control (IPC) has shown its potential to reduce structural loads, from numerical studies (Bossanyi, 2003) to experimental demonstrations (Bossanyi et al., 2013). In the mean time, several wind farm flow control strategies have been considered to mitigate wake effects and maximize power production in wind farms. Static flow control was originally proposed, mostly wake redirection using yaw control (Fleming et al., 2014; Wagenaar et al., 2012). Dynamic flow control has also been investigated, mostly the Pulse approach and the Helix approach. The first one, the Pulse, relies on Collective Pitch Control (CPC) to periodically vary the thrust force of the turbine, at a frequency that is typically one order of magnitude smaller than the turbine rotation frequency (Yilmaz and Meyers, 2018; Munters and Meyers, 2018). The resulting changes in induction generate pulsating patterns in the wake, which help it destabilize faster. When it comes to the Helix approach, IPC is used to generate sinusoidal variations of the tilt and yaw moments in quadrature phase (Frederik et al., 2020). As a consequence, the wake propagates downstream following the shape of a helix, and its recovery is enhanced (Korb et al., 2023). Both strategies come with additional loading and pitch bearing activity (Frederik and van Wingerden, 2022; van Vondelen et al., 2023b).

Let us focus the remainder of this review on pitch actuation-based control strategies, for which wind conditions awareness is often very limited. In the case of load alleviation using IPC, some studies proposed controllers including explicit information about the incoming wind, such as the rotor-effective wind speed measured by a LiDAR in Russell et al. (2024). Still, for most IPC controllers, the measurements used to determine the control actions are the blade loads (Bossanyi, 2003; Lu et al., 2015). When it comes to dynamic wake mixing, the Pulse and the Helix strategies act in an open-loop manner. In previous experimental and numerical contributions (van der Hoek et al., 2024; Korb et al., 2023; Taschner et al., 2023), the pitch actuation frequency is fixed for a studied configuration. It is computed based on the mean infinite upstream wind speed to match a chosen Strouhal number.

Yet refined wind conditions awareness could be essential to develop more efficient controllers (Meyers et al., 2022). When it comes to load alleviation, Selvam et al. (2009) showed that including a feedforward loop based on wind disturbance estimation in the IPC scheme further reduces structural loads. Russell et al. (2024) additionally demonstrated how LiDAR-assisted feedforward IPC was improving load alleviation results for turbines operating in freestream conditions. Coquelet et al. (2022) investigated the case of waked turbines and concluded that it provided challenges, calling for new IPC schemes accounting for partial or total wake impingement. When it comes to wake mixing, the controllers act in a dynamic way. How the actuation is phased with respect to turbulent structures in the incoming flow therefore influences their efficiency in alleviating wake effects. Munters and Meyers (2018) for instance showed, using an optimal control framework for dynamic induction control, that the vortex rings generated by the optimal controller coincide with bulges that are naturally present in the wake of the reference case. The turbine actuation thus phases itself with the incoming turbulent flow structures. van Vondelen et al. (2023a) and Korb et al. (2023) also showed, in the context of a line of three turbines, that the pitch phase offset between the first and the second turbine influences the power leveraged for the third turbine.

Though these examples highlight the potential of wind conditions awareness in the context of wind turbine and wind farm flow control, they still lack practical implementation due to sensing limitations. Anemometers have been present on nacelles for many years (Smith et al., 2002). Yet, they only provide information on the wind at the measurement point, making turbines unaware of wake impingement, shear or turbulent gusts. Their measurements additionally suffer from a number of disturbances resulting in unreliable measurements (Bottasso et al., 2018). Consequently, nacelle-mounted LiDARs have received growing attention, as they provide solutions to these limitations. They offer remote sensing and are able to provide a great characterization of the incoming flow. Most importantly, LiDARs are able to measure the incoming flow further upstream from the turbine, hence allowing the controller to prepare for future flow variations. For this reason, LiDARs are good candidates for feedforward control approaches (Letizia et al., 2023; Scholbrock et al., 2016). They are not a standard yet for modern turbines, likely due to their cost, complexity of installation, or need for synchronization with the SCADA system. However, their industrial use has been reported (Raach, 2021) and is likely to generalize in the future.

Alternative methods to characterize the inflow have also been investigated. They are based on the principle that any change in the wind is reflected on the load response of the rotor and that load sensors are now typically available for modern turbines (Cooperman and Martinez, 2015; Bottasso et al., 2018). This is referred to as the rotor-as-a-sensor approach, for which the structural response of the turbine is used to determine the wind conditions. Conversely to LiDARS, such approaches do not offer a preview of the future incoming wind, the estimation is limited to the current wind conditions. Several contributions on the topic rely on estimators deriving from Kalman filters. Simley and Pao (2016) present a linear Kalman filter-based estimator for estimation of hub-height wind speed and wind shear components. Interestingly, the authors show that the estimator performances degrade when blade pitch actuation occurs due to the nonlinearities appearing in the turbine response. Bottasso et al. (2018) introduce an extended Kalman filter (EKF) formulation to estimate blade-effective wind speeds. These are then transformed into sector-effective wind speeds for wake detection application. In Bertelè et al. (2017), this approach is extended to the estimation of inflow misalignment and shear angles through the identification of the blade load harmonics. The EKF approach is also reported in Lejeune et al. (2022), where the sensing is used to infer flow information to a meandering-capturing wake model developed for operational wind farm flow prediction. In Brandetti et al. (2023), it is an unscented Kalman filter that is used for blade-effective wind speed estimation on vertical-axis wind turbines. Other types of estimators have also been reported, such as a subspace predictive repetitive estimator in Liu et al. (2021) and both a proportional integral notch estimator and a Coleman-based estimator in Liu et al. (2022).

This work investigates the ability of these blade load-based estimators to infer the characteristics of the incoming wind when the turbine is operated with several advanced control strategies. Indeed, the underlying principle of load-alleviation IPC, the Pulse and the Helix is to use pitch actuation to modify blade loads. We wonder whether a blade load-based estimator can still be accurate in that context and therefore be used for closed-loop control applications. To answer this question, we deploy an EKF using the blade out-of-plane bending moments to estimate wind speed both at the rotor scale and at more local scales, building up on the work of (Bottasso et al., 2018). Kalman-filter based estimators rely on an internal model of the turbine relating the measurements and the estimations. Linearized models cover only a small range of turbine operation and lead to inaccuracies out of that range (Simley and Pao, 2016; van Vondelen et al., 2023a), while nonlinear look-up tables (Bottasso et al., 2018; Liu et al., 2021) cannot account for dynamic effects between actuation and loads. Regarding the dynamic pitching context is which this paper falls, we propose the use of a dynamic BEM formulation, covering the whole range of operation of the turbine and accounting for potential delays between pitch actuation and blade loads. We demonstrate the performance of the estimator using Large-Eddy Simulation (LES). The simulated blade bending moments and turbine operating parameters are fed to the estimator and the wind speed estimates are validated against the actual velocity field retrieved from the LES. We then verify the accuracy of the estimator in cases where pitch control strategies are active for load alleviation and for wake mixing.

The contributions are thus threefold:

1. Formulate a blade load-based estimator using a BEM as the internal model in the EKF.
2. Include dynamics in the BEM to account for delays between pitch action and blade loads in the context of dynamic pitch control.
3. Verify the robustness of this estimator to load alleviation and wake mixing control strategies in LES.

The remainder of the paper is organized as follows. Section 2 introduces the EKF and the testing environment. The performances of the estimator on a single turbine immersed in turbulent wind are assessed in Sec. 3. The robustness of the blade load-based estimator is evaluated for turbines using load alleviation and wake mixing control in Sec. 4. Eventually, conclusions are drawn alongside perspectives in Sec. 5.

2 Methodology

This section presents the structure of the blade load-based estimator and briefly describes the LES environment in which it is tested.

2.1 Extended Kalman Filter for wind speed estimation

The general procedure of the EKF theory is recalled before being applied to the estimation of blade-effective wind speeds. How the latter are then used to reconstruct several characteristics of the wind speed impinging on the rotor is eventually presented.

2.1.1 Extended Kalman Filter

Consider the discrete-time state-space representation of a nonlinear system

$$\boldsymbol{x}_k = \boldsymbol{f}\left(\boldsymbol{x}_{k-1}, \boldsymbol{u}_{k-1}\right) + \boldsymbol{w}_{k-1}, \tag{1}$$

$$\boldsymbol{y}_k = \boldsymbol{h}\left(\boldsymbol{x}_k, \boldsymbol{u}_k\right) + \boldsymbol{v}_k, \tag{2}$$

with $\boldsymbol{x}_k$ the state vector at time instant k, $\boldsymbol{y}_k$ the output or measurement vector, $\boldsymbol{u}_k$ the control input vector. $\boldsymbol{f}\left(\boldsymbol{x}_{k-1}, \boldsymbol{u}_{k-1}\right)$ is the nonlinear state function and $\boldsymbol{h}\left(\boldsymbol{x}_k, \boldsymbol{u}_k\right)$ is the measurement function. $\boldsymbol{w}_{\boldsymbol{k}}$ is the process noise vector and $\boldsymbol{v}_{\boldsymbol{k}}$ is the measurement noise vector. In EKF theory, they are assumed to be zero-mean Gaussian white noise with covariance matrices $\boldsymbol{Q}$ and $\boldsymbol{R}$, respectively (Chui et al., 2017).

The purpose of the EKF is to compute an estimate of the unknown states $\boldsymbol{x}$ based on the system model and input/output signals. It is an extension of the linear Kalman filter in the sense that it generalizes the formulation to nonlinear systems. To do so, it relies on the Jacobian matrices of the state and measurement functions, for the prediction and correction step respectively (Chui et al., 2017).

The prediction step at time k consists in computing the *a priori* error covariance estimate $\boldsymbol{P}_k^-$ and the *a priori* state estimate $\hat{\boldsymbol{x}}_k^-$, based on the previous estimates of the covariance matrix $\boldsymbol{P}_{k-1}^+$ and the state $\hat{\boldsymbol{x}}_{k-1}^+$, and the Jacobian matrix of the state function $\boldsymbol{F}_{k-1}$. The computation is as follows:

$$\boldsymbol{F}_{k-1} = \left.\frac{\partial \boldsymbol{f}}{\partial \boldsymbol{x}}\right|_{\hat{\boldsymbol{x}}_{k-1}^+,\boldsymbol{u}_{k-1}} \tag{3}$$

$$\boldsymbol{P}_k^- = \boldsymbol{F}_{k-1}\boldsymbol{P}_{k-1}^+\boldsymbol{F}_{k-1}^T + \boldsymbol{Q} \tag{4}$$

$$\hat{\boldsymbol{x}}_k^- = \boldsymbol{f}\left(\hat{\boldsymbol{x}}_{k-1}^+, \boldsymbol{u}_{k-1}\right)\ . \tag{5}$$

The correction step then makes use of the measurement $\boldsymbol{z}_k$ to compute the *a posteriori* state estimate $\hat{\boldsymbol{x}}_k^+$ and the *a posteriori* error covariance matrix $\boldsymbol{P}_k^+$, based on the Jacobian matrix of the measurement function $\boldsymbol{H}_k$, the measurement residual $\tilde{\boldsymbol{y}}_k$ and the Kalman gain $\boldsymbol{K}_k$. The procedure is as follows:

$$\boldsymbol{H}_k = \left.\frac{\partial \boldsymbol{h}}{\partial \boldsymbol{x}}\right|_{\hat{\boldsymbol{x}}_k^-,\boldsymbol{u}_k} \tag{6}$$

$$\boldsymbol{K}_k = \boldsymbol{P}_k^-\boldsymbol{H}_k^T\left(\boldsymbol{R} + \boldsymbol{H}_k\boldsymbol{P}_k^-\boldsymbol{H}_k^T\right)^{-1} \tag{7}$$

$$\boldsymbol{P}_k^+ = \left(\boldsymbol{I} - \boldsymbol{K}_k\boldsymbol{H}_k\right)\boldsymbol{P}_k^- \tag{8}$$

$$\tilde{\boldsymbol{y}}_k = \boldsymbol{z}_k - \boldsymbol{h}\left(\hat{\boldsymbol{x}}_k^-, \boldsymbol{u}_k\right) \tag{9}$$

$$\hat{\boldsymbol{x}}_k^+ = \hat{\boldsymbol{x}}_k^- + \boldsymbol{K}_k\tilde{\boldsymbol{y}}_k\ . \tag{10}$$

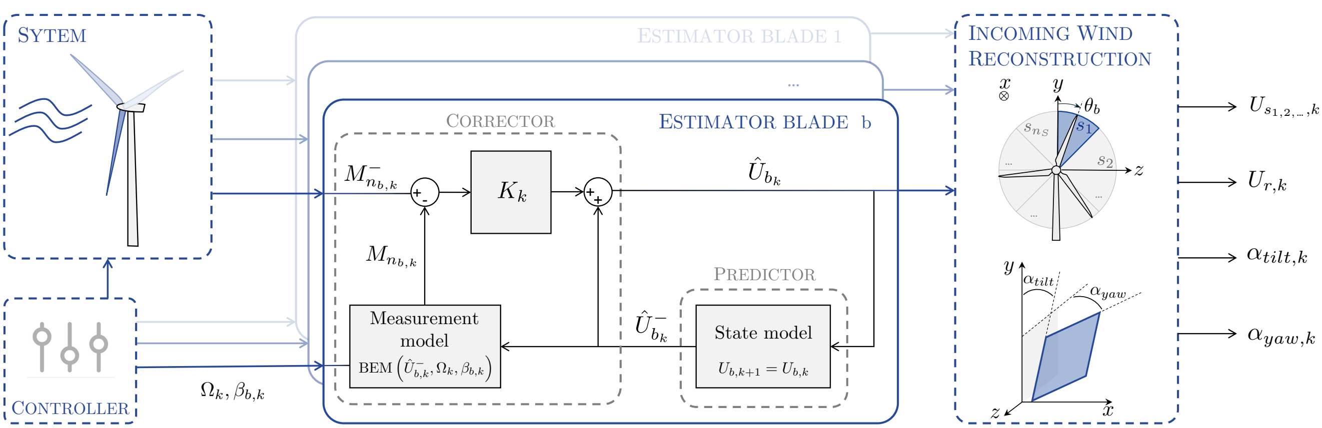

Figure 1. Block diagram of the blade load-based estimator relying on the BEM as internal model and on an extended Kalman filter as an estimator, each blade has its own estimator. The blade-effective wind speeds are mapped to the fixed frame in the wind reconstruction block.

2.1.2 Estimation of blade-effective wind speeds

We apply the EKF theory to the estimation of blade-effective wind speeds, considering blades as rotating sensors whose bending moments are measured. One estimation is performed for each blade b, as shown in the block diagram of Fig. 1.

Control input: The control input vector $\boldsymbol{u}$ consists in the rotation speed of the turbine and the blade pitch angle

$$\boldsymbol{u}_k = [\Omega_k, \beta_{b,k}]. \tag{11}$$

State: The variable to be estimated is the blade-effective wind speed, U_b, which is an input to the wind turbine blade system. To match the EKF formalism, we model this input as a state and do not explicitly model the internal states of the system. The one-dimensional state vector therefore writes

$$x_k = U_{b,k}\ . \tag{12}$$

State function: The state evolution is modeled as a random walk with process noise w:

$$U_{b,k} = f(U_{b,k-1}) + w_{k-1} = U_{b,k-1} + w_{k-1}\ . \tag{13}$$

Considering a random walk is equivalent to assuming that the estimated state is a bias, because the expected value is a constant. Using a random walk to model the evolution of the state is thus a simplification in this case, as the blade-effective wind speed is expected to be periodic with a 1P component. A model representation accounting for the 1P periodicity of the blade-effective wind speed as the one proposed in van Vondelen et al. (2023a) would better represent the system dynamics. Yet, the random walk was successfully used in the context of blade-effective wind speed estimation in Bottasso et al. (2018) and Brandetti et al. (2023), because the 1P variations are slow compared to the estimation time-step and can thus be captured.

Measurement function: The state is estimated based on the measurements of the blade out-of-plane bending moments, M_{n_b}. We model the system using the BEM theory, hence the nonlinear output equation is

$$M_{n_{b,k}} = h\left(U_{b,k}\ ,\ [\Omega_k, \beta_{b,k}]\right) + v_k \tag{14}$$

$$= \mathrm{BEM}\left(U_{b,k}\ ,\ [\Omega_k, \beta_{b,k}]\right) + v_k\ . \tag{15}$$

Note that the original version of the BEM theory is based on the conservation of momentum in a stream tube flowing through the rotor (Hansen, 2015). Therefore, it runs under the assumption of rotor-effective quantities. Appendix A shows how the BEM is used to return individual blade loads from blade-effective velocities. Another key assumption of the classical BEM theory, which we further refer to as static BEM, is that the wake is fully developed and that the induction of the rotor is then (quasi) steady (Hansen, 2015). In Sec. 4.3.2, we will show how this BEM model can be modified to account for the induction changes generated by the pitch control strategies considered in this paper.

Noise covariance matrices: Several combinations of process noise covariance and measurement noise covariance are tested to determine the best configuration. The values leading to the smallest estimation errors and avoiding excessive filtering are

$Q^* = Q/(U^*)^2 = 0.1$ and $R^* = R/(M_n^*)^2 = 0.0001$, where U^* and M_n^* represent the order of magnitude of the incoming wind speed and bending moments, respectively.

Jacobian matrices: The expression of the Jacobian matrix for the state function is trivial: $F_k = 1$.

As the BEM is an iterative method (see Appendix A), an analytical expression of the Jacobian matrix for the measurement function cannot be provided. We therefore numerically compute it using central finite differences, with ΔU a constant value tuned manually, following

$$H_k = \frac{h(\hat{U_b}_k^+ + \Delta U, [\Omega_k, \beta_{b,k}]) - h(\hat{U_b}_k^+ - \Delta U, [\Omega_k, \beta_{b,k}])}{2\Delta U}. \tag{16}$$

Note that this procedure requires two more BEM evaluations. Opting for forward finite differences, for example, could save one evaluation if computational time was to become an issue.

2.1.3 Reconstruction of the incoming wind

The procedure described above considers the estimation of the blade-effective wind speeds, that are naturally expressed in the blade rotating frame. They are further manipulated to provide information about the incoming flow in the fixed frame. We also want the information to be provided at a local scale, in order to capture turbulent and shear patterns in the wind. The rotor is then divided into a chosen number of sectors, n_S, and we map the blade-effective wind speeds to the sector-effective wind speeds (see Fig. 1). A sector-effective wind speed U_s is the mean blade-effective wind speed seen by the blade as it travels across a sector s. A sector-effective wind speed is updated every time a blade leaves that sector, i.e. at a 3P frequency. The update procedure is formally given in Appendix B. At every instant, the rotor-effective wind speed is computed as the average velocity of the n_S sectors.

The wind field can also be synthesized as a sheared plane (see Fig. 1). This provides a representation of the shear present in the atmospheric boundary layer through a tilting shear coefficient α_{tilt}, but also gust- or wake-generated shear in the yaw direction α_{yaw}. The least square approximation is used to find the expression of the plane best fitting the sector-effective wind speeds. Following derivations in Bottasso et al. (2018), sector-effective wind speeds are assumed to account for the wind speed at $r = 2R/3$. The target expression for the velocity field writes

$$U(y,z) = U_r + \alpha_{\text{tilt}}\, y + \alpha_{\text{yaw}}\, z, \tag{17}$$

with y the vertical direction and z the transverse one.

2.2 Simulation environment

The estimator is verified numerically. Simulations are performed with an in-house LES environment (Chatelain et al., 2017; Balty et al., 2020; Coquelet et al., 2022). The Navier-Stokes equations are solved by a Vortex Particle-Mesh method (Chatelain et al., 2013) and wind turbine blades are modeled by Immersed Lifting Lines (Caprace et al., 2019). The code is coupled to the multi-body-system solver ROBOTRAN that handles the dynamics of the rigid rotor (Docquier et al., 2013). Turbulence is injected at the inflow using Mann boxes (Mann, 1998). Wind shear can be modeled at the inflow through the power law

$$\frac{U(y)}{U_{\text{hub}}} = \left(\frac{y}{H_{\text{hub}}}\right)^{\alpha}, \tag{18}$$

where y is the vertical elevation from the ground, H_{hub} and U_{hub} are the hub height and velocity respectively, and α is the shear coefficient.

3 Validation of the estimator for a single turbine in turbulent flows with no shear

In this section, the estimator is validated for an isolated turbine operating in turbulent wind. The numerical setup is first presented, the results are then discussed.

3.1 Numerical setup

The estimator is validated using the NREL 5MW (Jonkman et al., 2009) wind turbine, characterized by a rotor diameter $D = 126$ m, a rated wind speed of 11.4 m/s and a rated rotor speed of 12.1 rpm. For this validation study, we consider three mean infinite upstream wind speeds U_{ref}: 5 m/s, 9 m/s and 14 m/s. For each wind speed, we consider three turbulence intensity (TI) levels: 6%, 10% and 15%. Shear is not present in these simulations and no controller is active: the turbine operates at a prescribed rotation speed and collective pitch angle following Jonkman et al. (2009).

The boundary conditions are inflow-outflow in the streamwise direction, x, and unbounded in the vertical, y, and transverse, z, directions. The extent of the computational domain is $8D \times 4D \times 4D$ with a $D/64$ spatial resolution. The LES time step is adaptive and the operating parameters of the turbine are sampled at a 10 Hz frequency to feed the EKF.

An adjunct LES in which no turbine is present is also performed for each wind case. The quantities estimated by the EKF can then be assessed by comparing them to the "ground truth", as the additional simulations provide an unambiguous definition of the freestream quantities. The rotor-effective wind speeds are computed as the average, over a disk located at the position of the rotor in the original simulation, of the streamwise velocity extracted from the adjunct LES. This is formally computed as

$$U_{r,k}^{\text{LES}} = \frac{1}{\pi R^2} \iint\limits_{\text{disk}} u_{x,k}(x = x_{WT}, y, z)\,\mathrm{d}S, \tag{19}$$

where $u_{x,k}$ is the streamwise velocity field at time k, x_{WT} is the location of the wind turbine in the original simulation and the spatial integral is performed over the disk area swept by the rotor blades. The formulation for the sector-effective wind speeds is similar, except for the fact that the spatial integral is performed over each sector area, such that

$$U_{s,k}^{\text{LES}} = \frac{n_S}{\pi R^2} \iint\limits_{\text{sector}} u_{x,k}(x = x_{WT}, y, z)\,\mathrm{d}S. \tag{20}$$

The tilt and yaw shear coefficients, $\alpha_{\text{tilt},k}^{\text{LES}}$ and $\alpha_{\text{yaw},k}^{\text{LES}}$ are retrieved from the sector-effective wind speeds using the least square fit approach as described in Eq. 17.

3.2 Results

The rotor is discretized into 8 sectors, providing an intermediate spatial resolution in the wind speed estimates. Figure 2 shows the estimation of the sector-effective wind speed (only one sector is shown for the sake of conciseness), the rotor-effective wind speed, and the tilt and yaw shear coefficients.

The temporal evolution of the sector-effective and rotor-effective wind speeds appears well captured across all simulations. The same remark holds for the shear coefficients. As expected, the estimated signals present steps, as a sector velocity is only updated when a blade leaves a sector, i.e. at a 3P frequency (see Appendix B). This update procedure is also partly responsible for the delay between the estimated velocities and the reference velocities. One can also notice that the estimates tend to deteriorate as the mean upstream wind speed decreases, this is discussed hereunder.

The estimator performances is quantified using the following indicators, with N_k the number of time steps:

$$\epsilon_{U_r}^{\text{abs}}\,[\%] = \frac{1}{N_k}\sum_k \frac{|U_{r,k} - U_{r,k}^{\text{LES}}|}{U_{\text{ref}}}\,, \tag{21}$$

$$\epsilon_{U_s}^{\text{abs}}\,[\%] = \frac{1}{n_S N_k}\sum_{s,k} \frac{|U_{s,k} - U_{s,k}^{\text{LES}}|}{U_{\text{ref}}}\,, \tag{22}$$

$$\epsilon_{U_s}\,[\%] = \frac{1}{n_S N_k}\sum_{s,k} \frac{U_{s,k} - U_{s,k}^{\text{LES}}}{U_{\text{ref}}}\,, \tag{23}$$

$$\epsilon_{\alpha_{\text{yaw}}}[\%] = \frac{1}{N_k}\sum_k \frac{|\alpha_{\text{yaw},k} - \alpha_{\text{yaw},k}^{\text{LES}}|}{\frac{1}{2}\left(\max_k \alpha_{\text{yaw},k}^{\text{LES}} - \min_k \alpha_{\text{yaw},k}^{\text{LES}}\right)}\,, \tag{24}$$

$$\epsilon_{\alpha_{\text{tilt}}}[\%] = \frac{1}{N_k}\sum_k \frac{|\alpha_{\text{tilt},k} - \alpha_{\text{tilt},k}^{\text{LES}}|}{\frac{1}{2}\left(\max_k \alpha_{\text{tilt},k}^{\text{LES}} - \min_k \alpha_{\text{tilt},k}^{\text{LES}}\right)}\,. \tag{25}$$

Regarding the estimation of the rotor-effective velocity, the relative absolute errors reported in Tab. 1 remain under 4%, while for the sector-effective velocities, they remain under 5%. This is similar to the errors in Bottasso et al. (2018).

We also verify whether a bias is present in the estimation by computing ϵ_{U_s}. Table 1 shows that a bias around 0.3% is present for $U_{\text{ref}} = 15$ m/s and it increases to become of the order of $2 - 2.5\%$ for $U_{\text{ref}} = 5$ m/s. This reveals that a mismatch appears between the internal model of the estimator, the BEM, and the actual system, the LES, as the wind speed decreases. It is known from the literature that the 1D momentum theory from which the BEM is derived breaks down at low wind speeds as the rotor is heavily loaded (Hansen, 2015). As the EKF procedure consists in comparing the real output of the system to the expected output computed by the model, a bias in the model leads to a bias in the estimation.

U_{ref} [m/s]	5			9			15		
TI [%]	6	10	15	6	10	15	6	10	15
$\epsilon_{U_r}^{\mathrm{abs}}$ [%]	2.2	2.6	3.6	1.7	3.1	3.1	0.5	0.8	1.7
$\epsilon_{U_s}^{\mathrm{abs}}$ [%]	2.5	3.4	4.9	2.1	4.6	4.5	1.0	1.8	3.0
ϵ_{U_s} [%]	2.3	2.5	3.3	1.4	2.5	1.7	0.2	0.3	0.5
$\epsilon_{\alpha_{\mathrm{yaw}}}$ [%]	6.1	7.9	6.6	5.8	14.9	6.7	4.2	4.9	4.9
$\epsilon_{\alpha_{\mathrm{tilt}}}$ [%]	8.0	7.9	7.7	7.6	9.5	7.6	5.2	5.1	5.6

Table 1. Relative errors for the estimation of the rotor-effective wind speed, the sector-effective wind speed and the shear coefficients for the 9 validation cases.

While the absolute level of the forces is higher in the LES than in the BEM, hence the positive bias in the estimation, the dynamic changes of the system state are well captured (see Fig. 2). The estimator thus entails a great perception of the temporal and local changes in wind speed, which is what is of most interest for the control purposes targeted in this paper. Would the bias still be an issue, a bias-aware EKF could be used, as suggested by Drécourt et al. (2006). A common practice is to augment the state vector of the original problem with the bias (Friedland, 1969). The EKF therefore estimates both the state and the bias, as done in the work of Pamososuryo et al. (2023) in the context of wind turbine control.

Table 1 also reveals a degradation of the error metrics as TI increases. We relate this to the spatio-temporal averaging underlying the estimation process. The reference sector-effective wind speed is the unweighted average of the flow field in the radial and azimuthal directions. The sector-effective wind speed estimated by the EKF is also the result of an averaging, but performed differently. First, the radial averaging is materialized by the blade-effective wind speed. The latter is computed by the EKF as to minimize the difference between the measured bending moment (here extracted from LES) and the modeled bending moment (here obtained from the BEM). So the EKF uses the BEM to synthesize a turbulent wind speed distribution into a single blade-effective wind speed. Yet a wind turbine blade, and as a consequence the BEM, is nonlinear. Therefore the radial averaging is not simply an unweighted average. Second, the azimuthal averaging is performed by the transformation from blade-effective wind speed to sector-effective wind speed. Every azimuthal information considered to get the sector-average corresponds to a different instant and the estimated sector-effective wind speed is only updated at a 3P frequency. This is the limitation of using discrete blades as sensors. To summarize, the reference sector-effective wind speed at time t is a linear combination of local wind speeds at time t, while the estimated sector-effective wind speed at time t is a non linear combination of local wind speeds from time $t - T_{\mathrm{rot}}/3$ to t. If the flow field was uniform, the averaging performed by the estimator would be equivalent to the reference averaging. But as turbulence increases, the output of the spatio-temporal averaging associated with the estimator diverges from the reference one.

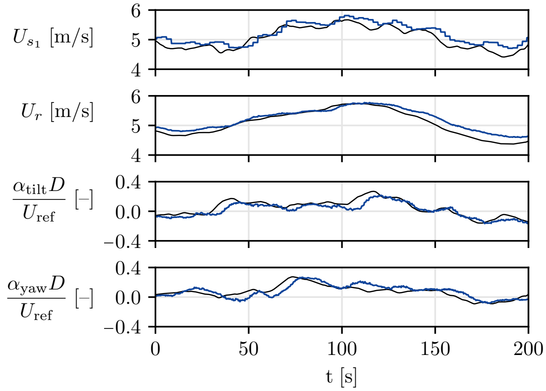

(a) $U_{\mathrm{ref}} = 5$ m/s, $\Omega_{\mathrm{rot}} = 7.5$ rpm, $\beta = 0^{\mathrm{o}}$

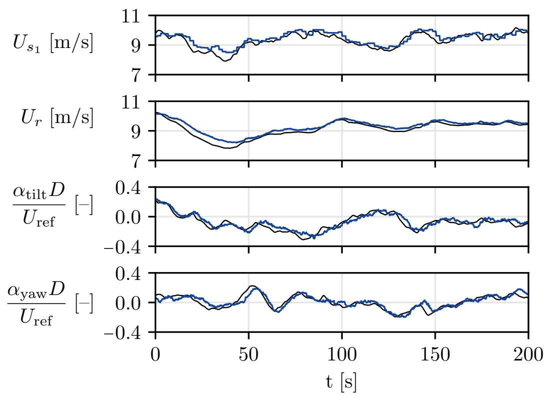

(b) $U_{\mathrm{ref}} = 9$ m/s, $\Omega_{\mathrm{rot}} = 10.3$ rpm, $\beta = 0^{\mathrm{o}}$

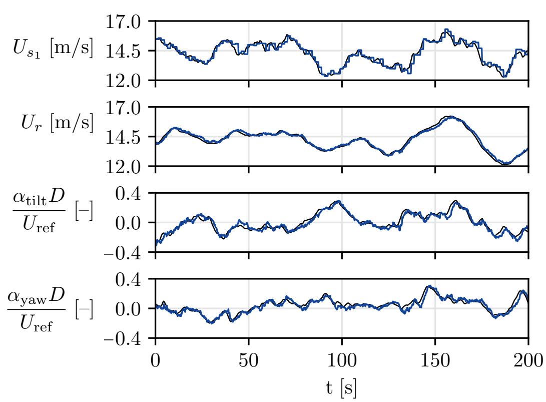

(c) $U_{\mathrm{ref}} = 14$ m/s, $\Omega_{\mathrm{rot}} = 12.1$ rpm, $\beta = 8.7^{\mathrm{o}}$

Figure 2. Estimated wind characteristics (sector-effective wind speed, rotor-effective wind speed, shear coefficients) at three wind speeds with $\mathrm{TI} = 10\%$: LES-recovered references (black) and estimated values (blue).

4 Robustness of the estimator to active pitch control strategies

While the previous section has focused on validating the estimator, this section aims at testing it in more realistic wind conditions and when controllers are active on the turbine. The choice of the study cases is motivated hereunder.

4.1 Controllers

The estimator presented here relies on blade loads and operating parameters. Both are influenced by the controller that is active on the wind turbine. In this section, we verify that the estimator is robust to the chosen control strategy. To do so, we propose simulations in which the three following pitch control strategies are considered: individual pitch control for load alleviation, individual pitch control for wake mixing and collective pitch control for wake mixing. The implementation of these controllers is presented hereafter.

A Baseline controller is active in all cases and serves as a comparison for the other cases. It is a classical implementation of a variable-speed, variable-pitch controller (Jonkman et al., 2009). It relies on generator torque control, maximizing the power captured below the rated wind speed, and CPC, regulating the collective pitch angle β_{coll} to maintain nominal power production above the rated wind speed.

For the controllers relying on individual pitch actions, the Coleman transform is used to map fixed-frame pitch commands to rotating-frame ones (Bossanyi, 2003). The individual blade pitch angles $\beta_{1,2,3}$ are retrieved from the fixed-frame pitch angles, β_{tilt} and β_{yaw}, and the collective pitch angle β_{coll}, based on the inverse Coleman transform:

$$\begin{bmatrix} \beta_1 \\ \beta_2 \\ \beta_3 \end{bmatrix} = \begin{bmatrix} 1 & \cos\theta & \sin\theta \\ 1 & \cos\left(\theta - \frac{2\pi}{3}\right) & \sin\left(\theta - \frac{2\pi}{3}\right) \\ 1 & \cos\left(\theta + \frac{2\pi}{3}\right) & \sin\left(\theta + \frac{2\pi}{3}\right) \end{bmatrix} \begin{bmatrix} \beta_{\text{coll}} \\ \beta_{\text{tilt}} \\ \beta_{\text{yaw}} \end{bmatrix},$$

where θ is the azimuthal position of the first blade ($\theta = 0$ when the blade is pointing upward).

The IPC-based load alleviation controller, further referred to as IPC, consists of two PI controllers, one for the yaw axis and one for the tilt axis. They compute the fixed-frame pitch commands $\beta_{\text{tilt,yaw}}$ bringing the fixed-frame loads $M_{\text{tilt,yaw}}$ to zero, in the fashion of Bossanyi (2003). More details on this specific implementation can be found in Coquelet et al. (2020).

The IPC-based wake mixing controller, further referred to as Helix, is implemented as an open-loop control strategy (Frederik et al., 2020). It imposes sinusoidal variations of the fixed-frame pitch angles, namely $\beta_{\text{tilt}} = A\sin(2\pi f_p\, t)$ and $\beta_{\text{yaw}} = A\cos(2\pi f_p\, t)$. The frequency f_p is defined by the Strouhal number $St = f_p D/U_{\text{ref}}$, based on the rotor diameter D and the wind speed U_{ref}. The pitch actuation generates variations of the tilt and yaw moments, eventually forcing the wake to displace laterally and vertically (see Fig. 3) and to propagate downstream as a helix, hence the name.

The CPC-based wake mixing controller generates a pulsing pattern in the wake (see Fig. 3) by periodically changing the thrust force of the rotor. The position of the wake is not impacted, but its intensity and expansion change over time as a result of the changes in induction. We further refer to this strategy as the Pulse. It is implemented as a superimposition of low-frequency harmonic oscillations onto the collective pitch angle $\beta_{\rm coll}$ computed by the baseline controller. The pitch angles evolution is thus dictated by

$$\beta_1 = \beta_2 = \beta_3 = \beta_{\rm coll} + A\sin\left(2\pi St \frac{U_{\rm ref}\, t}{D}\right). \tag{26}$$

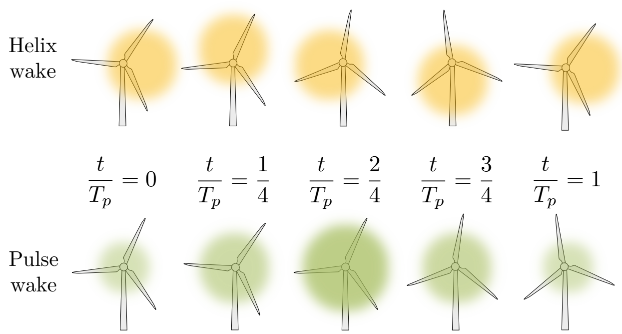

Figure 3. Simplified representation and description, over a period T_p, of the Helix (yellow) and Pulse (green) wakes impinging on a downstream wind turbine. The colored zone schematically represents the wake deficit, the opacity reflects its intensity while the radius reflects its expansion.

4.2 Numerical setups

We perform the LES of a pair of in-line NREL 5MW turbines with a $5D$ spacing (Fig. 4(a)), such that the estimator can be tested on a freestream turbine but also on a waked turbine. The boundary conditions are inflow-outflow in the streamwise direction x, slip wall in the vertical direction y, and periodic in the transverse direction z. The numerical domain extent is $12D \times 3D \times 8D$, the spatial resolution is $D/32$.

The inflow wind is sheared ($\alpha = 0.2$) and turbulent ($TI = 6\%$), in order to represent atmospheric boundary layer flows. Two wind speeds are considered: 9 m/s and 14 m/s. For the 9 m/s cases, both turbines operate in under-rated conditions: this is representative of a configuration in which wake mixing control would be applied. On the first turbine, we therefore test the Baseline controller, the Pulse, the Helix and IPC for the sake of completeness, even though it is usually not used at below-rated wind speeds. The downstream turbine is always operated using the Baseline controller. We opt for commonly used parameters for both the Helix and the Pulse (Frederik et al., 2020; Munters and Meyers, 2018): $St = 0.25$ and $A = 2.5^{\rm o}$. Note that, as both turbines operate at under-rated wind speed, only the generator torque control is active for the Baseline controller, such that the collective pitch control $\beta_{\rm coll} = 0$. For the 14 m/s cases, both turbines operate in above-rated conditions. There would be no point in using wake mixing control in that case, hence it is not tested. Conversely, this is a configuration in which both the upstream and downstream turbines would use load alleviation control. We therefore consider two cases: Baseline controller on both turbines and IPC on both turbines. In both cases, collective pitch control is used by the Baseline controller for power

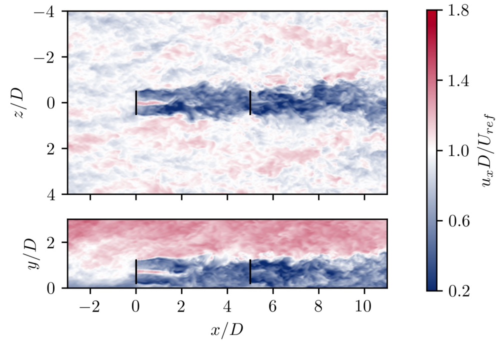

(a) Simulation used to retrieve the operating parameters and bending moments on the two turbines.

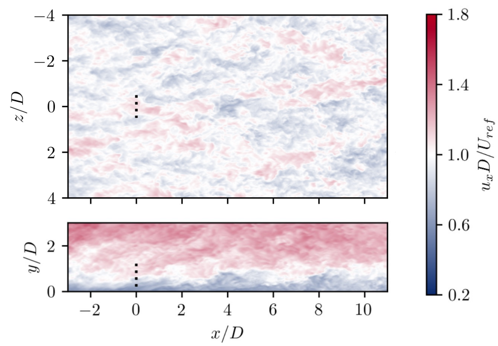

(b) Simulation used to compute reference wind speeds for the upstream turbine.

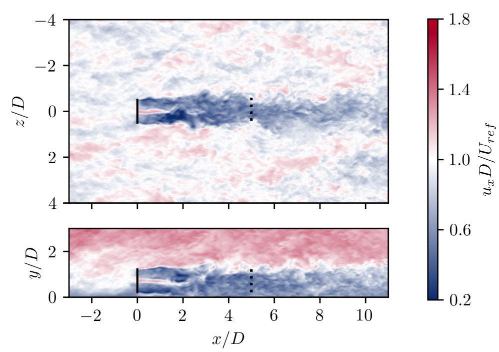

(c) Simulation used to compute reference wind speeds for the downstream turbine.

Figure 4. Horizontal and vertical slices of the instantaneous streamwise velocity field used to retrieve bending moments to feed the estimator (a), and simulations used as reference to verify the wind speeds estimates for the first (b) and second (c) turbines. Only the 9 m/s Baseline control case is shown.

regulation. When load alleviation control is switched on, the individual pitch commands are added on top of the collective pitch command, following the Coleman transform. Table 2 summarizes the above-mentioned cases.

9 m/s		14 m/s	
WT1	WT2	WT1	WT2
Baseline	Baseline	Baseline	Baseline
IPC	Baseline	IPC	IPC
Helix	Baseline		
Pulse	Baseline		

Table 2. Summary of the configurations tested to investigate the robustness of blade-load based estimator to active pitch control.

The wind speed estimation for both the upstream and the downstream turbine is performed at a 10 Hz frequency. For the upstream one, the reference velocities is defined as the velocity from a slice located at the rotor position when the rotor is not present (Fig. 4(b)). When it comes to the downstream turbine, the reference velocities are accordingly retrieved from simulations of each control case in which only the first turbine is present (Fig. 4(c)). The reference velocities are computed following Eq. 19 and Eq. 20.

4.3 Under-rated conditions: 9 m/s

The under-rated condition cases are discussed in this section. The impact of the control strategy is first highlighted, then a adaptation of the BEM accounting for dynamic pitch actuation is proposed and results for the upstream and downstream turbines are presented.

4.3.1 Impact of the control strategy on operating parameters and measured loads

Figure 5 shows the impact of the controller on the operating parameters and the out-of-plane moments. The Baseline case shows that, if the pitch is equal for all blades, the effect of shear and turbulence generates 1P oscillations (period T_{rot}) on the blade bending moments.

When IPC is used, the changes in wind speed perceived by the blade as it rotates are compensated by the pitch actuation. These vary individually at the 1P frequency, the amplitude of the actuation varies with time as the controller operates in closed loop.

For the Pulse, all blades are pitched at the same angle. Given the Strouhal number of 0.25, the actuation period T_p is about ten times the rotation period. The amplitude of the pitch oscillations is constant as the strategy is open-loop. The mean value of the out-of-plane moments is marked by this periodicity and displays the changes in rotor induction.

For the Helix case, it comes from the Coleman transform that the pitching frequency is $1/T_{\mathrm{rot}} + 1/T_p$ (see Frederik et al. (2020) for derivation), while the pitching amplitude is constant. This does not impact the mean value of the bending moments,

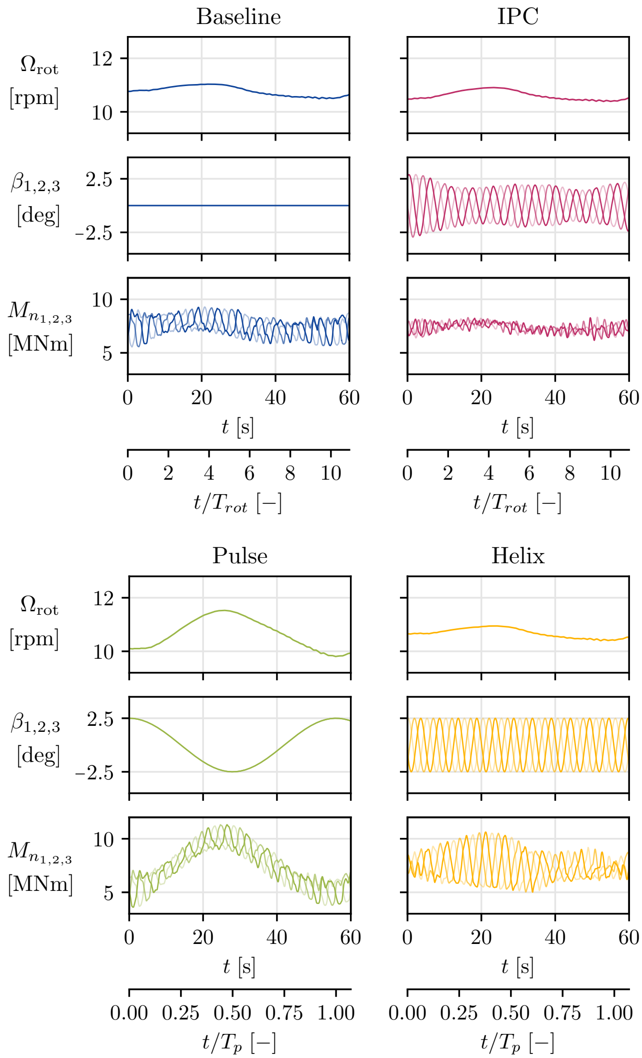

Figure 5. Effect of the control strategy on rotation speed, blade pitch angles, and out-of-plane bending moment. One color shade is used for each blade. The time axis is given in seconds and rotation periods T_{rot} for the Baseline and IPC controllers as the dominant effects are observed at 1P in those cases. For the Pulse and the Helix, time is made dimensionless using the actuation period T_p.

as the individual pitch action is performed in a three-phase manner, with a 120º offset between each blade. Rather, the effect is also visible on the amplitude of the bending moments, which is sometimes increased (around $t = 20$ s in Fig. 5) and sometimes decreased (around $t = 50$ s in Fig. 5). The effect is better understood looking at tilt and yaw moments, as those become quadrature phase sinusoidal signals with a $1/T_p$ frequency.

This section has highlighted how the control strategies considered in this work impact the state of the turbine, i.e. its operating parameters and the loads it experiences. This further motivates the need to verify the robustness of the blade load-based estimator to the pitch control strategy active on the turbine. It also points at verifying the accuracy of the BEM in scenarios that involve dynamic actuation.

4.3.2 Handling effects of dynamic actuation in the BEM

In the current formulation of the estimator, the internal model relies on the BEM theory. As discussed before, the standard BEM maps the operating parameters of the turbine and the wind speed to the forces exerted on the blades, and the mapping is static. This comes from the assumption of the BEM that the wake is fully developed, which underlies that the induction of the blades and thus the induced velocities around them are (quasi) steady. Yet the Pulse and the Helix inherently generate periodic variations of the induction, hence the wake is never fully developed. Through the collective pitch actuation, the Pulse changes the induction of the entire rotor. When it comes to the Helix, the individual pitch actuation changes the local induction of each blade. A time delay therefore exists before equilibrium is reached between the induction factors and the aerodynamic loads. In order to account for it, we propose to make use of a dynamic formulation for the BEM, based on the work of Snel and Schepers (1995). Appendix A presents how the quasi-steady normal, a, and tangential, a', induction factors are computed. From these induction factors, the quasi-steady induced velocities, normal w_n and tangential w_t, are recovered as $\boldsymbol{w}_{\text{qs}} = [w_n, w_t] = [aU_0, a'\Omega_{\text{rot}} r]$, where U_0 is the infinite upstream velocity and r is the local radius of the considered blade section (see Fig. A1).

Following Snel and Schepers (1995), the induced velocities are filtered with the following first-order differential equations

$$\boldsymbol{w}_{\text{int}} + \tau_1 \frac{\mathrm{d}\boldsymbol{w}_{\text{int}}}{\mathrm{d}t} = \boldsymbol{w}_{\text{qs}} + k_1 \tau_1 \frac{\mathrm{d}\boldsymbol{w}_{\text{qs}}}{\mathrm{d}t}, \tag{27}$$

$$\boldsymbol{w} + \tau_2 \frac{\mathrm{d}\boldsymbol{w}}{\mathrm{d}t} = \boldsymbol{w}_{\text{int}}, \tag{28}$$

where $\boldsymbol{w}_{\text{int}}$ is a working variable, $k_1 = 0.6$ is a constant and τ_1 and τ_2 are time constants.

The corrected induction factors are retrieved from the corrected induced velocities $\boldsymbol{w} = [w_n, w_t]$ following

$$[a,\ a'] = [w_n/U_0,\ w_t/(\Omega_{\text{rot}}\, r)]. \tag{29}$$

We further refer to the BEM without dynamic effects as the static BEM and to the one enhanced with dynamic effects as the dynamic BEM. The tunable time constants τ_1 and τ_2 for the dynamic BEM are calibrated against LES data. To do so, we perform the simulation of the NREL 5MW in uniform inflow with no shear at $U_{\text{ref}} = 9$ m/s when the Pulse and the Helix are active. The turbine rotation speed and blade pitch angles determined by the controller in the LES framework are retrieved and fed to the static and dynamic BEM. We recall that the Immersed Lifting Line method used to compute aerodynamic forces in the LES intrinsically accounts for dynamic effects in the induction and is thus the reference.

Figure 6 compares, over one period T_p, the BEM values with those provided by the LES for the local induction and the out-of-plane bending moment.

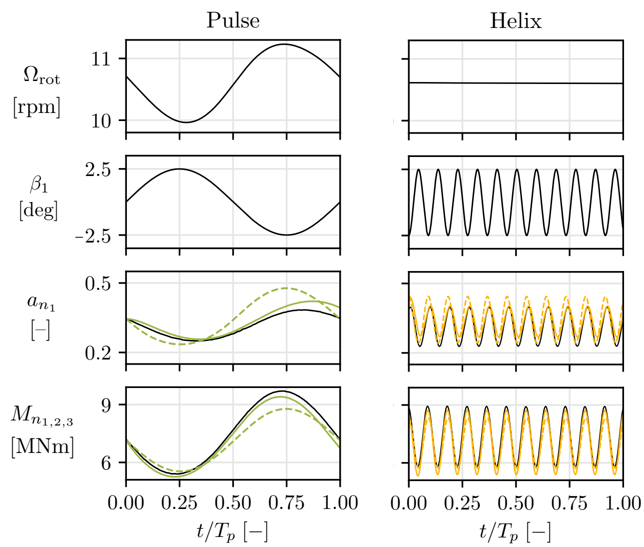

Figure 6. Comparison of LES (solid black), static BEM (dashed colored) and dynamic BEM (solid colored) in the evaluation of the local forces acting on the airfoil located at $r/R = 3/4$ for the NREL 5MW operated in uniform flow with $U_{\text{ref}} = 9$ m/s.

It shows that, with the static BEM, the axial induction is in direct phase opposition with the pitch angle. It behaves as if, as soon as the pitch angle increases, the induced velocities are reduced. When considering the dynamic effects, a certain delay appears, which is different for the Pulse and the Helix.

Based on the analytical expression provided in Hansen (2015), we propose the following tuning of the time constants:

$$\tau_1 = \frac{1}{7(1-1.3\,a)}\,\frac{1}{f_{\text{pitch}}}\,, \tag{30}$$

$$\tau_2 = \left(0.39 - 0.26\left(\frac{r}{R}\right)^2\right)\tau_1\,, \tag{31}$$

with R, the rotor radius.

TSR being the tip speed ratio, we recall that the pitching frequency of the blade f_{pitch} is

$$f_{\text{pitch}}^{\text{Pulse}} = f_p = St\,\frac{U_{\text{ref}}}{D} \tag{32}$$

$$f_{\text{pitch}}^{\text{Helix}} = f_{\text{rot}} + f_p = \left(\frac{\text{TSR}}{\pi} + St\right)\frac{U_{\text{ref}}}{D}\,. \tag{33}$$

This section therefore shows that ignoring the delays leads to poor evaluation of the angle of attack, which eventually leads to inaccurate loads. Including dynamic effects in the BEM therefore increases the accuracy of the internal model of the estimator, which should improve the quality of the estimate provided by the EKF.

4.3.3 Results for the upstream turbine

We divide the rotor into four sectors ($n_S = 4$) placed as a cross, which leads to a top, right, bottom, and left sector. This allows us to capture the effects of shear thanks to the top-bottom differences and the effects of gust or wake impingement through the left-right imbalances. We first comment the results of the estimator in its original formulation, i.e. using the static BEM. Time series of the rotor-effective and sector-effective wind speeds are provided in Fig. 7, along with their Power Spectral Density (PSD).

When it comes to the rotor-effective wind speed, the estimations are almost identical for the Baseline, IPC and Helix cases. When the Pulse is active on the turbine, oscillations appear in the wind speed estimate at the Pulse frequency. For the sector-effective wind speed, these oscillations are present not only for the Pulse but also for the Helix.

This highlights that neglecting the dynamic effects in the internal model of the system, as it is done with the look-up table approaches in Bottasso et al. (2018), Liu et al. (2021) or Liu et al. (2022), is inadequate for the considered application. When the static BEM is used, the expected measurement provided by the internal model in the EKF is not accurate. There is a mismatch with the actual measurement, and the wind speed estimate is wrongfully corrected in the correction step. For the Pulse, this leads to periodic oscillations of both the rotor-effective wind speed and the sector-effective wind speed at the actuation frequency $1/T_p$. With the Helix control, the changes of induction are performed individually at each blade in a three-phase manner, with a 120$^{\text{o}}$ offset between each blade. The inaccurate oscillations therefore appear on the blade-effective wind speeds, but they cancel out at the rotor scale.

Figure 7 presents the result of the estimators once dynamics is taken into account in the internal BEM model. The estimates are now identical whatever the control strategy active on the turbine: the adapted estimator is robust to the control strategy. The capacities of the estimator described in Sec. 3 and demonstrated by several studies in the literature are then retrieved. The estimator is able to recover the higher velocities in the top sector, the intermediate ones in the left and right sectors, and the lower ones in the bottom sector. It is thus able to capture turbulence, shear, gusts, etc. The estimation errors are reported in Table 3 and are close to 5%.

	Baseline	IPC	Pulse	Helix
$\epsilon^{\text{abs}}_{U_r}$ [%]	5.2	4.7	4.9	4.9
$\epsilon^{\text{abs}}_{U_s}$ [%]	5.4	5.0	5.2	5.2
ϵ_{U_s} [%]	5.4	4.9	5.1	5.1

Table 3. 9 m/s case: Wind speed estimation errors for the upstream turbine (WT1).

The overestimation bias discussed in Sec. 3 is also observed, yet it is around 5% here, while it was around $1.5-2\%$ in the validation case at the same 9 m/s wind speed. We attribute this increase in bias to the setup used for the simulations. Indeed, to maintain affordable computational costs, the spatial resolution used for the LES is coarsen to $D/32$, while the resolution

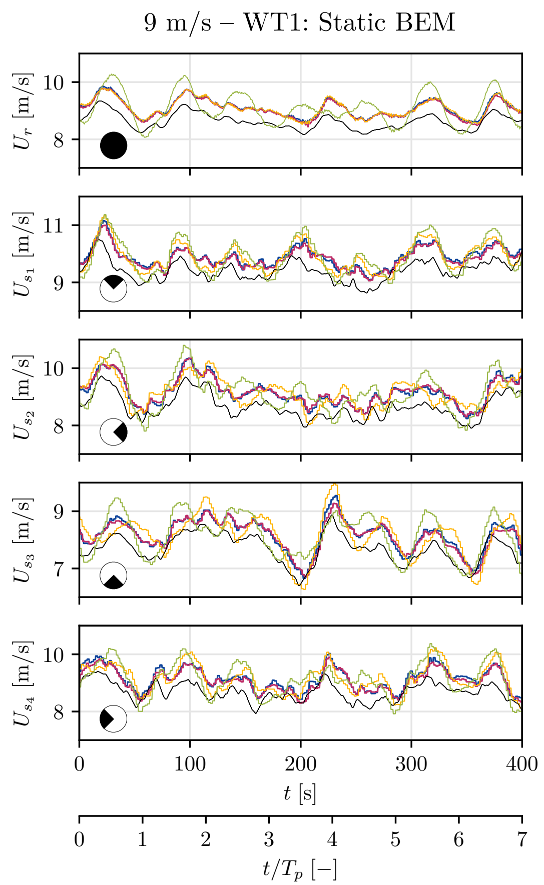

(a) Time series of the estimated wind speeds using static BEM.

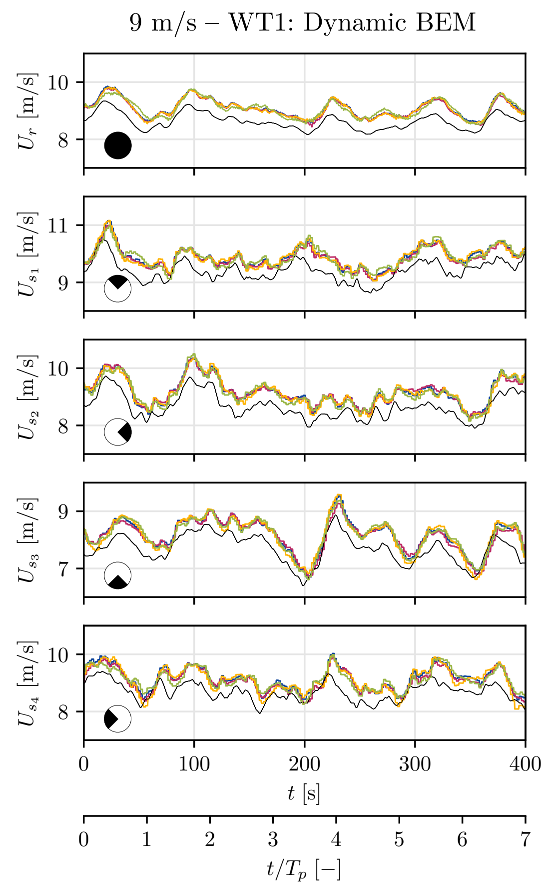

(b) Time series of the estimated wind speeds using dynamic BEM.

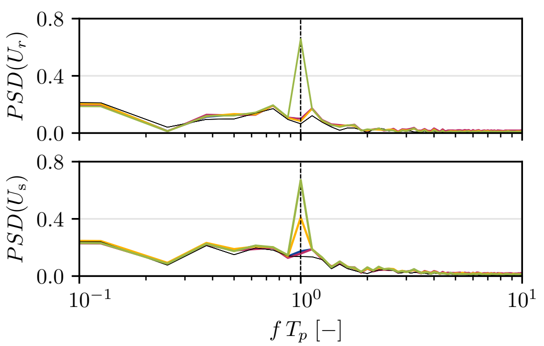

(c) Power spectral density of the time series using static BEM.

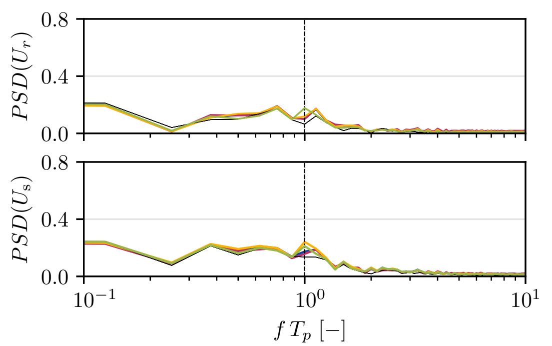

(d) Power spectral density of the time series using dynamic BEM.

Figure 7. 9 m/s case: Wind speed estimation on the upstream turbine (WT1) using a static (left) and dynamic (right) BEM as the internal model in the EKF. Reference velocities (black) are extracted from the LES. The wind speeds are estimated by the upstream turbine which is operated with four different control strategies: Baseline (blue), IPC (red), Pulse (green) and Helix (yellow).

was twice finer in Sec. 3. It is known that the forces computed by the LES increase when the resolution decreases due to poor capture of the tip losses (Moens et al., 2018). The mismatches between the internal model (BEM) and the actual system (LES) is higher with the simulations in this section than with those from Sec. 3. In the correction step, the EKF therefore corrects the velocity to a higher value than it should. As suggested before, this could be corrected with bias estimation (Friedland, 1969).

4.3.4 Results for the downstream turbine

The Pulse and the Helix are wake mixing control strategies, which means that their purpose is to modify the wake. Namely, the Pulse is expected to generate a pulsing sequence in the wake, with alternating zones of lower and higher velocities, while the Helix laterally and vertically displaces the wake as it propagates downstream (see Fig. 3). In this section, we want to verify the performances of the estimator in waked flows and its ability to capture the frequency content added to the wake by the Pulse and the Helix.

Figure 8(a) shows that the estimator performs reasonably well in waked conditions, capturing the large-scale changes in the wind. Yet, the estimation somewhat deteriorates compared to the upstream turbine case, as Table 4 reports. Two reasons can be mentioned to support the bigger discrepancies and stem from the inherent characteristics of a wind turbine wake: reduced velocity and higher turbulence. On the one hand, the flow dynamics is harder to capture due to the complexity and randomness of turbulence. On the other hand, the BEM loses accuracy at lower velocity, hence the bigger bias present in the estimation (6% on average against the 5% for the freestream turbine).

Figure 8(b) shows that the estimator is able to capture the frequency content added to the wake by the Pulse and the Helix control strategies. Looking back at the time series, it is also interesting to notice that the phase at which higher and lower velocity flow parcels are impacting a sector, or the rotor, is properly captured. This is an interesting result from the perspective of applying the Helix or the Pulse to deeper lines of turbines. The downstream turbine could therefore also be actuated with the Helix or the Pulse. To do so in an optimal way, it should synchronize its action with the periodic perturbations already present in the wake, as proposed in van Vondelen et al. (2023a) or Korb et al. (2023).

	Baseline	IPC	Pulse	Helix
$\epsilon_{U_r}^{\text{abs}}$ [%]	6.4	6.2	6.6	5.8
$\epsilon_{U_s}^{\text{abs}}$ [%]	7.0	6.9	7.3	6.6
ϵ_{U_s} [%]	6.6	6.4	6.7	6.0

Table 4. 9 m/s case: Wind speed estimation errors for the downstream turbine (WT2). The controller refers to the controller that is active on the upstream turbine. The downstream turbine is always operated with Baseline control.

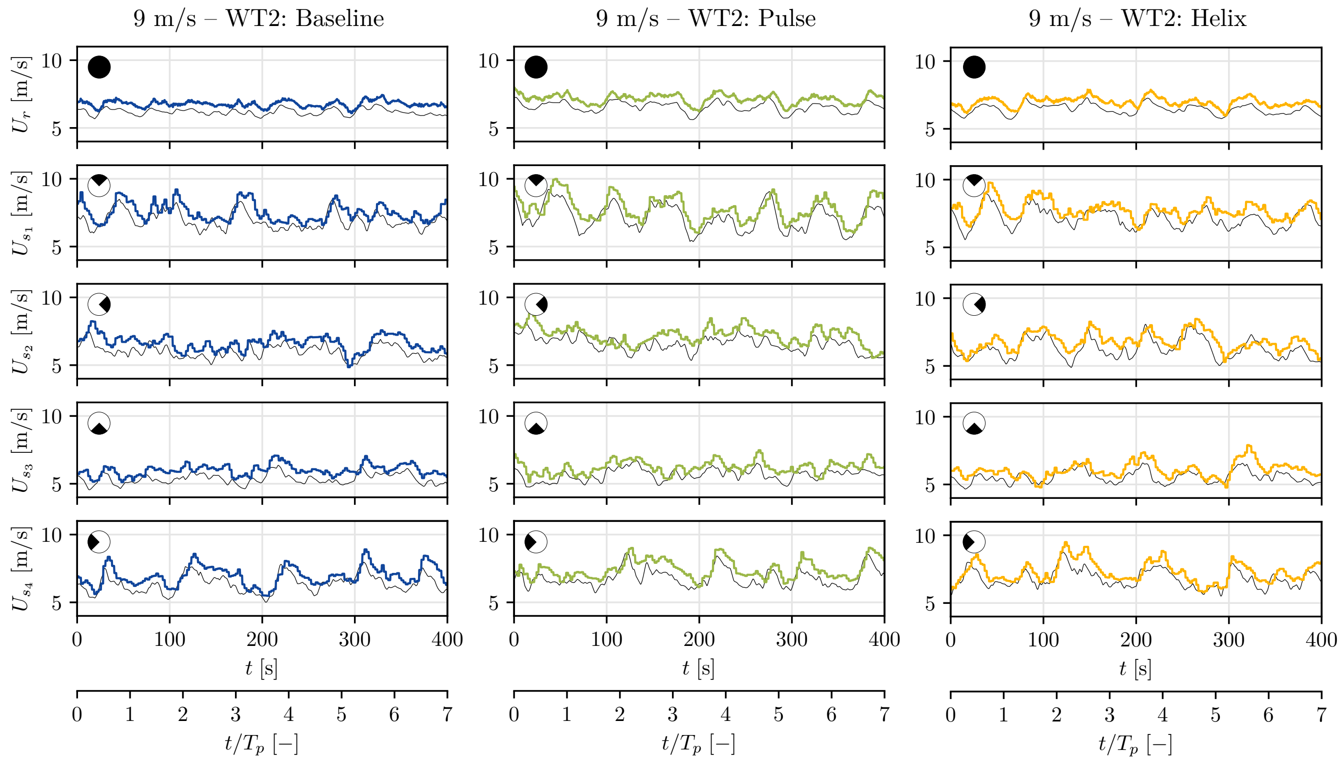

(a) Time series of the estimated wind speeds.

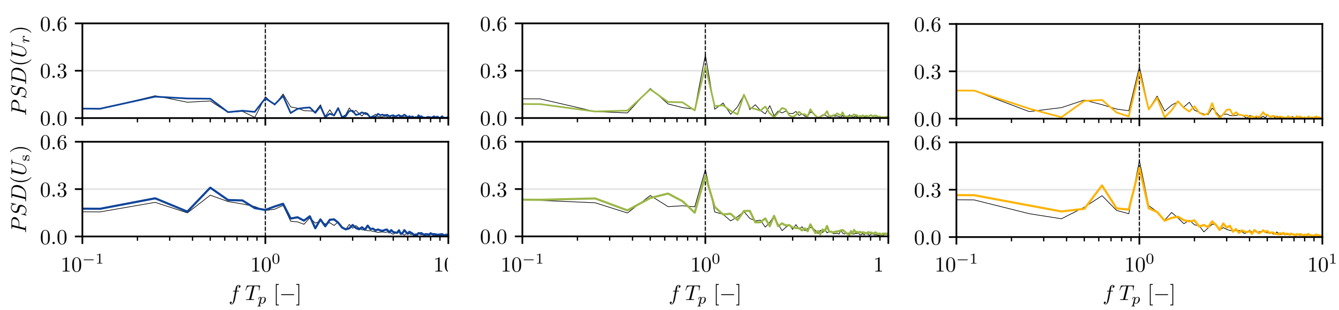

(b) Power spectral density (PSD) of the time series.

Figure 8. 9 m/s case: Wind speed estimation on the downstream turbine (WT2), operated with Baseline control, using a static BEM as internal model in the EKF. Reference velocities (black) are extracted from the LES with the sole upstream turbine operated with four different control strategies: Baseline (blue), Pulse (green) and Helix (yellow).

4.4 Above-rated conditions: 14 m/s

This final section discusses the above-rated wind speed cases. The impact of using IPC on the pitch angle and blade loads was highlighted in Fig. 5 and is not shown here anymore. Note however that CPC is active in these wind conditions. Figure 9

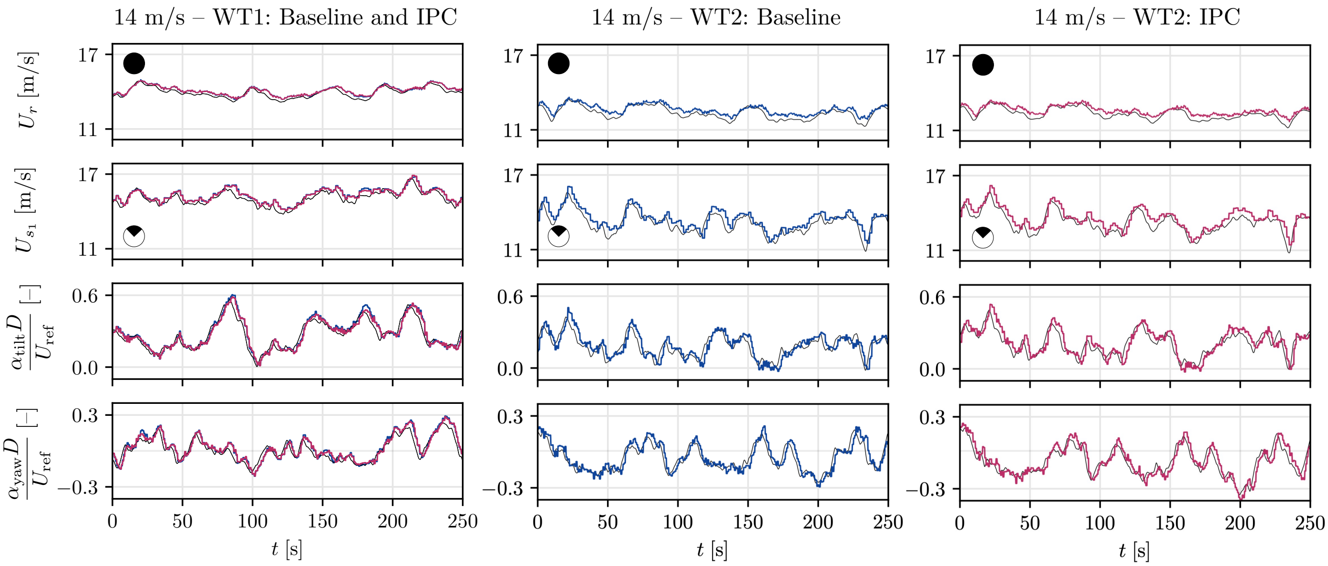

Figure 9. 14 m/s case: Time series of estimated wind speeds for both turbines (WT1 and WT2), using a static BEM as internal model in the EKF. Reference velocities (black) are extracted from the LES, both turbines are either operated with Baseline (blue) or IPC (red).

shows the time series of the wind speed estimates for the two turbines. The static BEM is used as internal model. Separate subfigures are used for the downstream turbine as the wake is somewhat different whether IPC is used on the upstream turbine or not (Wang et al., 2020). The reference wind speed is thus slightly different for the two cases, as it can be observed when carefully looking at Fig. 9. Instead of showing all sector-effective wind speeds as in the previous sections, Figure 9 rather presents the horizontal and vertical shear coefficient (Eq. 17), as these quantities are specifically insightful for load alleviation control using IPC.

First, results show that the static BEM is sufficient in these cases. CPC for power regulation is active in the Baseline case and additional individual pitching is added on top of it in the IPC case. Still, no rapid changes in induction are associated with the two control cases, hence the static BEM is accurate to model the link between operating parameters, wind speed and blade bending moments. Figure 9 also shows that the bias of the estimator is reduced, both for the freestream and the waked turbine. This is quantitatively confirmed by Table 5, which shows that errors remain under 3% for the estimated wind speeds. It is a direct consequence of the higher wind speed: the BEM is more accurate at reduced thrust coefficients and the estimation is better.

Time series also show a good capture of the shear coefficients. The vertical wind shear of the inflow is sensed (α_{tilt} is non zero on average), while the horizontal shear generated by turbulent gusts is also seen (α_{yaw} varies around a zero mean).

	Baseline WT1	IPC WT1	Baseline WT2	IPC WT2
$\epsilon^{\text{abs}}_{U_r}$ [%]	1.4	1.4	1.8	1.8
$\epsilon^{\text{abs}}_{U_s}$ [%]	2.0	2.0	2.5	2.6
ϵ_{U_s} [%]	1.5	1.5	1.9	2.0
$\epsilon_{\alpha_{\text{tilt}}}$ [%]	11.0	10.9	20.2	20.7
$\epsilon_{\alpha_{\text{yaw}}}$ [%]	17.7	17.1	17.7	16.1

Table 5. 14 m/s case: Wind speeds and shear coefficients estimation errors for the two turbines (WT1 and WT2). The latter are either both operated with Baseline control or with IPC.

5 Conclusions

This work assesses the ability of a blade load-based wind speed estimator to accurately sense the characteristics of the incoming wind when both collective and individual pitch control is active at the turbine.

The proposed estimator relies on Extended Kalman filter, whose internal model of the system is based on the BEM theory. When power regulation CPC and load alleviation IPC are used, a state-of-the-art static BEM ensures accurate wind speed estimations by the EKF. What this paper highlights is that, when wake mixing control is used, it is needed to account for dynamic changes in blade induction. Indeed, the static BEM is not an accurate model when the Pulse or the Helix are active on the turbine, as the static BEM considers an immediate reaction of the blade loads to the pitch actuation. It ignores the unsteady effects in the wake related to the changes in induction. Including an unsteady correction in the model is the solution we propose to make the EKF robust to the controller active on the turbine. This contribution is essential if the EKF is to be used for state-feedback control, the application targeted for this tool.

Indeed, using IPC for load alleviation in complex wind conditions is still challenging and could benefit from explicit information on local wind speeds and global shear coefficients provided by the estimator. For the Pulse and the Helix controllers, sensing the incoming flow is needed for them to be used in a closed-loop manner. This would allow them to optimally phase their dynamic actuation with the dynamics of the incoming flow structures. When talking about an upstream turbine, this refers to the gusts and shear of the atmospheric boundary layer. When talking about a waked turbine, this also refers to synchronization with the added periodic content in the Helix and Pulse wakes. A direct follow-up to this work then consists in determining if the precision provided by this estimator is sufficient for these control applications, which might lead to having to deal with the bias of the estimator. This also comes along with finding a control formulation including the wind speed estimates.

Another perspective is to investigate the effects of blade flexibility on the proposed estimator. The structural dynamics of the rotor are indeed not considered in this study, as both the EKF estimator and the LES simulations assume a rigid rotor. Accounting for blade flexibility modifies the blade root moments in three ways: mean value, amplitude of the fluctuations and phase of the fluctuations (Trigaux et al., 2024b). And these effects increase as the rotor diameter increases (Trigaux et al., 2024a). Further investigations are thus needed in that field, especially when the estimator is used for larger rotors.

Appendix A: Blade Element Momentum theory

The BEM used in this work was implemented in-house following Hansen (2015) and validated against FAST. Rotor tilt and blade cone angle are not taken into account, the rotor is considered as a flat disk perpendicular to the inflow. Algorithm A1 highlights the key steps of the BEM computation. The latter is performed in an iterative manner until the value of the flow angle ϕ [rad] is converged with a tolerance $\mathrm{tol} = 10^{-6}$ in this case. Flow angle and other quantities of interest for the BEM are illustrated in Fig. A1. The Glauert correction is used for high induction and, when needed, dynamic effects can be taken into account (see Sec. 4.3.2). We refer to Hansen (2015) for more details.

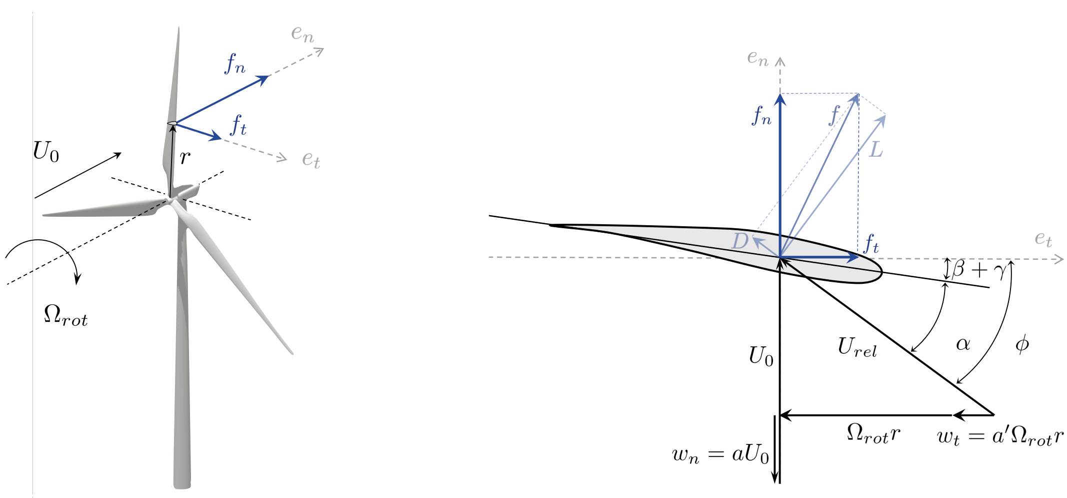

(a) Reference frame for the forces computation

(b) Velocity triangle at a cross-section of the blade

Figure A1. Quantities of interest in the BEM computation

Algorithm A1 BEM

for Each blade section **do**

Radial position r, chord c

Initialize induction factors and flow angle

$$a = 0.5, \quad a' = 0.005, \quad \phi_{\text{new}} = \pi/2, \quad \phi_{\text{old}} = \pi/2 + 1$$

while $\phi_{\text{new}} - \phi_{\text{old}} > \text{tol}$ **do**

$$\phi_{\text{old}} = \phi_{\text{new}}$$

Compute angle of attack and relative velocity

$$U_n = (1-a)\, u_0, \quad U_t = (1+a')\, \Omega_{\text{rot}} r$$

$$\phi = \tan^{-1}(U_n/U_t)$$

$$\alpha = \phi - (\beta + \gamma)$$

$$U_{\text{rel}} = \sqrt{U_n^2 + U_t^2}$$

Retrieve lift and drag coefficients from polar

$$C_L = C_L(\alpha), \quad C_D = C_D(\alpha)$$

Compute normal and tangential force coefficients

$$C_n = C_L \cos\phi + C_D \sin\phi, \quad C_t = C_L \sin\phi - C_D \cos\phi$$

Compute new induction factors

$$F_{\text{tip}} = \frac{2}{\pi} \arccos\left(\exp\left(-n_B \frac{R - r}{2r\sin\phi}\right)\right)$$

$$F_{\text{hub}} = \frac{2}{\pi} \arccos\left(\exp\left(-n_B \frac{r - R_{\text{hub}}}{2r\sin\phi}\right)\right)$$

$$\sigma = \frac{n_B c}{2\pi r}$$

$$a = \frac{1}{\dfrac{4F\sin^2\phi}{\sigma C_n} + 1}$$

$$a' = \frac{1}{\dfrac{4F\sin\phi\cos\phi}{\sigma C_t} - 1}$$

Update flow angle

$$\phi_{\text{new}} = \phi$$

end while

Compute local tangential and normal force

$$f_n = \tfrac{1}{2}\rho U_{\text{rel}}^2 c C_n, \quad f_t = \tfrac{1}{2}\rho U_{\text{rel}}^2 c C_t$$

end for

Integrate over span to compute out-of-plane bending moment of blade b

$$M_{n,b} = \int_{R_{\text{hub}}}^{R_{\text{tip}}} (r - R_{\text{hub}})\, f_{n,b}\, dr$$

Appendix B: From blade-effective wind speed to sector-effective wind speed

The rotor swept area is divided into n_S sectors of azimuthal span $\Delta\theta = 2\pi/n_S$. Algorithm B1 formalizes the conversion from blade-effective wind speed ($U_{b,k}$) to sector-effective wind-speed ($U_{s,k}$) for a rotor with n_B blades. The second subscript stands for the time index k. The process is initiated at $k = 1$ for each blade b by determining the sector $s_{b,k=1}$ in which the blade is located based on its azimuthal position $\theta_{b,k=1}$. The time-history of the blade-effective wind speed is then accumulated as the blade passes through the sector using the counting variable nit_b. The wind speed of sector s is eventually updated when the blade leaves the sector $s_b = s$. While the blade-effective wind speeds are updated at every time index k, i.e. at the EKF estimation frequency (0.1 s in this work), the sector-effective wind speeds are only updated at a 3P frequency (around 2 s) in this context.

Algorithm B1 Transforming blade-effective wind speeds to sector-effective wind speeds

---

initialization at time instant $k = 1$
  $U_{s,k=1} = 0 \quad \forall\, s$
  $\mathrm{nit}_b = 1 \quad \forall\, b$
  $s_{b,k=1} = \mathrm{integer}\,(\theta_{b,k=1}/\Delta\theta) \quad \forall\, b$
while estimation is ongoing **do**
  $U_{s,k} \leftarrow U_{s,k-1} \quad \forall\, s$
  for b in n_B **do**
    $s_{b,k} = \mathrm{integer}\,(\theta_{b,k}/\Delta\theta)$
    if $s_{b,k} \neq s_{b,k-1}$ **then**
      $s^* = s_{b,k-1}$
      $U_{s^*,k} \leftarrow \frac{1}{\mathrm{nit}_b} \sum_{\kappa=k-\mathrm{nit}_b}^{k-1} U_{b,\kappa}$
      $\mathrm{nit}_b \leftarrow 1$
    else
      $\mathrm{nit}_b \leftarrow \mathrm{nit}_b + 1$
    end if
  end for
end while

Author contributions. MC, ML, PC and LB worked at conceptualizing this research and establishing the methodology. MC and ML developed the BEM and EKF software. MC set up, ran and postprocessed the LES. AV and JWW provided feedback on the methodology. MC prepared the original draft with contribution from all authors, which was then reviewed by all authors. PC, LB and JWW provided funding.

Competing interests. At least one of the (co-)authors is an Associate editor of Wind Energy Science.

Acknowledgements. This project has received funding from the European Research Council under the European Union's Horizon 2020 research and innovation program (grant agreement no. 725627) and from the Université de Mons under the 50/50 PhD funding program. This work is also part of Hollandse Kust Noord wind farm innovation program where CrossWind C.V., Shell, Eneco, Grow and Siemens Gamesa are teaming up; funding for the PhD's and PostDocs was provided by Cross- Wind C.V. and SiemensGamesa.

This research benefited from computational resources made available on the Tier-1 supercomputer of the Fédération Wallonie-Bruxelles, infrastructure funded by the Walloon Region under the grant agreement no. 1117545. Computational resources were also provided by the Consortium des Equipements de Calcul Intensif, funded by the Fonds de la Recherche Scientifique de Belgique under Grant No. 2.5020.11 and by the Walloon Region.

References

Balty, P., Caprace, D.-G., Waucquez, J., Coquelet, M., and Chatelain, P.: Multiphysics simulations of the dynamic and wakes of a floating Vertical Axis Wind Turbine, Journal of Physics: Conference Series, https://doi.org/10.1088/1742-6596/1618/6/062053, 2020.

Bertelè, M., Bottasso, C., Cacciola, S., Daher Adegas, F., and Delport, S.: Wind inflow observation from load harmonics, Wind Energy Science, 2, 615–640, https://doi.org/10.5194/wes-2-615-2017, publisher: Copernicus GmbH, 2017.

Bossanyi, E.: Individual blade pitch control for load reduction, Wind Energy, https://doi.org/10.1002/we.76, 2003.

Bossanyi, E., Fleming, P., and Wright, A.: Validation of individual pitch control by field tests on two-and three-bladed wind turbines, IEEE Transactions on Control Systems Technology, https://doi.org/10.1109/TCST.2013.2258345, 2013.

Bottasso, C., Cacciola, S., and Schreiber, J.: Local wind speed estimation, with application to wake impingement detection, Renewable Energy, https://doi.org/10.1016/j.renene.2017.09.044, 2018.

Brandetti, L., Liu, Y., Pamososuryo, A., Mulders, S., Watson, S., and van Wingerden, J.W.: Unscented Kalman filter-based blade-effective wind speed estimation for a vertical-axis wind turbine, IFAC-PapersOnLine, 56, 8393–8399, https://doi.org/10.1016/j.ifacol.2023.10.1033, 2023.

Caprace, D.-G., Chatelain, P., and Winckelmans, G.: Lifting line with various mollifications: theory and application to an elliptical wing, AIAA Journal, https://doi.org/10.2514/1.J057487, 2019.

Chatelain, P., Backaert, S., Winckelmans, G., and Kern, S.: Large Eddy Simulation of Wind Turbine Wakes, Flow, Turbulence and Combustion, https://doi.org/10.1007/s10494-013-9474-8, 2013.

Chatelain, P., Duponcheel, M., Caprace, D.-G., Marichal, Y., and Winckelmans, G.: Vortex particle-mesh simulations of vertical axis wind turbine flows: from the airfoil performance to the very far wake, Wind Energy Science, https://doi.org/10.5194/wes-2-317-2017, 2017.

Chui, C., Chen, G., et al.: Kalman filtering, Springer, 2017.

Cooperman, A. and Martinez, M.: Load monitoring for active control of wind turbines, Renewable and Sustainable Energy Reviews, 41, 189–201, https://doi.org/https://doi.org/10.1016/j.rser.2014.08.029, 2015.

Coquelet, M., Bricteux, L., Lejeune, M., and Chatelain, P.: Biomimetic individual pitch control for load alleviation, Journal of Physics: Conference Series, https://doi.org/10.1088/1742-6596/1618/2/022052, 2020.

Coquelet, M., Bricteux, L., Moens, M., and Chatelain, P.: A reinforcement-learning approach for individual pitch control, Wind Energy, https://doi.org/10.1002/we.2734, 2022.

Docquier, N., Poncelet, A., and Fisette, P.: ROBOTRAN: A powerful symbolic gnerator of multibody models, Mechanical Sciences, https://doi.org/10.5194/ms-4-199-2013, 2013.

Drécourt, J.-P., Madsen, H., and Rosbjerg, D.: Bias aware Kalman filters: Comparison and improvements, Advances in Water Resources, 29, 707–718, https://doi.org/10.1016/j.advwatres.2005.07.006, 2006.

Fleming, P., Gebraad, P., Lee, S., van Wingerden, J.W., Johnson, K., Churchfield, M., Michalakes, J., Spalart, P., and Moriarty, P.: Evaluating techniques for redirecting turbine wakes using SOWFA, Renewable Energy, https://doi.org/10.1016/j.renene.2014.02.015, 2014.

Frederik, J. and van Wingerden, J.W.: On the load impact of dynamic wind farm wake mixing strategies, Renewable Energy, https://doi.org/10.1016/j.renene.2022.05.110, 2022.

Frederik, J., Doekemeijer, B., Mulders, S., and van Wingerden, J.W.: The helix approach: Using dynamic individual pitch control to enhance wake mixing in wind farms, Wind Energy, https://doi.org/10.1002/we.2513, 2020.

Friedland, B.: Treatment of bias in recursive filtering, IEEE Transactions on Automatic Control, 14, 359–367, https://doi.org/10.1109/TAC.1969.1099223, 1969.

Hansen, M.: Aerodynamics of wind turbines, Routledge, 2015.

Jonkman, J., Butterfield, S., Musial, W., and Scott, G.: Definition of a 5-MW reference wind turbine for offshore system development, National Renewable Energy Lab, 2009.

Korb, H., Asmuth, H., and Ivanell, S.: The characteristics of helically deflected wind turbine wakes, Journal of Fluid Mechanics, 965, A2, https://doi.org/10.1017/jfm.2023.390, 2023.

Lejeune, M., Moens, M., and Chatelain, P.: A meandering-capturing wake model coupled to rotor-based flow-sensing for operational wind farm flow prediction, Frontiers in Energy Research, https://doi.org/10.3389/fenrg.2022.884068, 2022.

Letizia, S., Brugger, P., Bodini, N., Krishnamurthy, R., Scholbrock, A., Simley, E., Porté-Agel, F., Hamilton, N., Doubrawa, P., and Moriarty, P.: Characterization of wind turbine flow through nacelle-mounted lidars: a review, Frontiers in Mechanical Engineering, 9, https://doi.org/10.3389/fmech.2023.1261017, 2023.

Liu, Y., Pamososuryo, A., Ferrari, R., Hovgaard, T., and van Wingerden, J.W.: Blade effective wind speed estimation: A subspace predictive repetitive estimator approach, in: 2021 European Control Conference (ECC), pp. 1205–1210, IEEE, https://doi.org/10.23919/ECC54610.2021.9654981, 2021.

Liu, Y., Pamososuryo, A., Mulders, S., Ferrari, R., and van Wingerden, J.W.: The proportional integral notch and Coleman blade effective wind speed estimators and their similarities, IEEE Control Systems Letters, 6, 2198–2203, https://doi.org/10.1109/LCSYS.2021.3140171, 2022.

Lu, Q., Bowyer, R., and Jones, B.: Analysis and design of Coleman transform-based individual pitch controllers for wind-turbine load reduction, Wind Energy, 2015.

Mann, J.: Wind field simulation, Probabilistic Engineering Mechanics, https://doi.org/10.1016/S0266-8920(97)00036-2, 1998.

Meyers, J., Bottasso, C., Dykes, K., Fleming, P., Gebraad, P., Giebel, G., Göçmen, T., and van Wingerden, J.W.: Wind farm flow control: prospects and challenges, Wind Energy Science, https://doi.org/10.5194/wes-2022-24, 2022.

Moens, M., Duponcheel, M., Winckelmans, G., and Chatelain, P.: An actuator disk method with tip-loss correction based on local effective upstream velocities, Wind Energy, https://doi.org/10.1002/we.2192, 2018.

Munters, W. and Meyers, J.: Towards practical dynamic induction control of wind farms: analysis of optimally controlled wind-farm boundary layers and sinusoidal induction control of first-row turbines, Wind Energy Science, https://doi.org/10.5194/wes-3-409-2018, 2018.

Pamososuryo, A., Liu, Y., Gybel Hovgaard, T., Ferrari, R., and van Wingerden, J.W.: Convex economic model predictive control for blade loads mitigation on wind turbines, Wind Energy, 26, 1276–1298, https://doi.org/10.1002/we.2869, 2023.

Raach, S.: Important milestone: 1000 wind turbines with lidar-assisted control, Sowento, https://www.sowento.com/wp-content/uploads/2021/11/20210527-sowento-PressRelease-Goldwind.pdf, 2021.

Russell, A., Collu, M., McDonald, A., Thies, P., Keane, A., and Quayle, A.: LIDAR-assisted feedforward individual pitch control of a 15 MW floating offshore wind turbine, Wind Energy, n/a, https://doi.org/10.1002/we.2891, 2024.

Scholbrock, A., Fleming, P., Schlipf, D., Wright, A., Johnson, K., and Wang, N.: Lidar-enhanced wind turbine control: Past, present, and future, in: 2016 American Control Conference (ACC), pp. 1399–1406, IEEE, https://doi.org/10.1109/ACC.2016.7525113, 2016.

Selvam, K., Kanev, S., van Wingerden, J.W., van Engelen, T., and Verhaegen, M.: Feedback–feedforward individual pitch control for wind turbine load reduction, International Journal of Robust and Nonlinear Control, https://doi.org/10.1002/rnc.1324, 2009.

Simley, E. and Pao, L.: Evaluation of a wind speed estimator for effective hub-height and shear components, Wind Energy, 19, 167–184, https://doi.org/10.1002/we.1817, 2016.

Smith, B., Link, H., Randall, G., and McCoy, T.: Applicability of nacelle anemometer measurements for use in turbine power performance tests, Tech. rep., National Renewable Energy Laboratory (NREL), 2002.

Snel, H. and Schepers, J.: Joint investigation of dynamic inflow effects and implementation of an engineering method, in: 1993 ECWEC Conference, ECWEC, 1995.

Taschner, E., van Vondelen, A., Verzijlbergh, R., and van Wingerden, J.W.: On the performance of the helix wind farm control approach in the conventionally neutral atmospheric boundary layer, Journal of Physics: Conference Series, 2505, 012 006, https://doi.org/10.1088/1742-6596/2505/1/012006, 2023.

Trigaux, F., Chatelain, P., and Winckelmans, G.: Investigation of blade flexibility effects over the loads and wake of a 15 MW wind turbine using a flexible actuator line method, Wind Energy Science Discussions, 2024, 1–33, https://doi.org/10.5194/wes-2024-19, 2024a.

Trigaux, F., Chatelain, P., and Winckelmans, G.: Investigation of blade flexibility effects over the loads and wake of a 15 MW wind turbine using a flexible actuator line method, Wind Energy Science Discussions, 2024, 1–33, https://doi.org/10.5194/wes-2024-19, 2024b.

United Nations: Transforming our world: the 2030 Agenda for Sustainable Development, https://wedocs.unep.org/20.500.11822/9814, 2015.

van der Hoek, D., den Abbeele, B. V., Simao Ferreira, C., and van Wingerden, J.-W.: Maximizing wind farm power output with the helix approach: Experimental validation and wake analysis using tomographic particle image velocimetry, Wind Energy, 27, 463–482, https://doi.org/10.1002/we.2896, 2024.

van Vondelen, A., Ottenheym, J., Pamososuryo, A., Navalkar, S. T., and van Wingerden, J.W.: Phase Synchronization for Helix Enhanced Wake Mixing in Downstream Wind Turbines, IFAC-PapersOnLine, 56, 8426–8431, https://doi.org/10.1016/j.ifacol.2023.10.1039, 2023a.

van Vondelen, A. A. W., Navalkar, S. T., Kerssemakers, D. R., and Van Wingerden, J.W.: Enhanced wake mixing in wind farms using the Helix approach: A loads sensitivity study, in: 2023 American Control Conference (ACC), pp. 831–836, https://doi.org/10.23919/ACC55779.2023.10155965, 2023b.

Wagenaar, J., Machielse, L., and Schepers, J.: Controlling wind in ECN's scaled wind farm, Proc. Europe Premier Wind Energy Event, 2012.

Wang, C., Campagnolo, F., and Bottasso, C.: Does the use of load-reducing IPC on a wake-steering turbine affect wake behavior?, Journal of Physics: Conference Series, https://doi.org/10.1088/1742-6596/1618/2/022035, 2020.

Yilmaz, A. and Meyers, J.: Optimal dynamic induction control of a pair of inline wind turbines, Physics of Fluids, https://doi.org/10.1063/1.5038600, 2018.